의학박사 학위논문

Neuronal mechanisms of cocaine sensitization : Rewiring of prelimbic cortex to nucleus accumbens connections

코카인 민감화의 신경회로 기전 : 중격의지핵으로 가는 전변연 시냅스 입력의 변화

2023년 2월

서울대학교 대학원

의과학과 생리학 전공

권 재 한

코카인 민감화의 신경회로 기전 : 중격의지핵으로 가는 전변연 시냅스 입력의 변화

지도 교수 호 원 경

이 논문을 의학박사 학위논문으로 제출함
2022년 10월

서울대학교 대학원
의과학과 생리학 전공
권 재 한

권재한의 의학박사 학위논문을 인준함
2023년 1월

위 원 장 이 석 호 (인)

부위원장 호 원 경 (인)

위 원 이 용 석 (인)

위 원 김 정 훈 (인)

위 원 강 웅 구 (인)

Neuronal mechanisms of cocaine sensitization : Rewiring of prelimbic cortex to nucleus accumbens connections

By Jaehan Kwon

A thesis submitted to the Department of Physiology
in partial fulfillment of the requirements
for the Degree of Doctor of Philosophy
at the Seoul National University College of Medicine

January 2023

Approved by Thesis Committee:

Chair Suk-Ho Lee (인)

Vice Chair Won-Kyung Ho (인)

Examiner Yong-Seok Lee (인)

Examiner Joung Hun Kim (인)

Examiner Ung Gu Kang (인)

Abstract

The medial prefrontal cortex (mPFC) has diverse projection targets and these targets are divided into 2 groups according to developmental criteria, group of extra-telencephalic region (ET) and group of intra-telencephalic region. The pyramidal neurons (PNs) in PFC have different physiological properties depending on whether the projecting target is ET or IT region. Especially, persistent sodium current ($I_{Na,P}$) dependent persistent activity is frequently occurred in ET cell while less observed in IT cell. Like this, $I_{Na,P}$ plays a key role in generating and maintaining repetitive firing, however, cell type specific study of contribution of $I_{Na,P}$ on excitability is lacking. Using retrograde tracing and patch clamp technique, I compared intrinsic properties and $I_{Na,P}$ amplitude between ET and IT cell. Furthermore, I modulated $I_{Na,P}$ and identified change of intrinsic excitability by using riluzole, $I_{Na,P}$ blocker. As a result, ET- and IT cells had different intrinsic properties including sag ratio, input resistance and intrinsic excitability. $I_{Na,P}$ amplitude of ET cell was larger than those of IT cell. Decreased $I_{Na,P}$ by riluzole reduced intrinsic excitability of both ET and IT cell, but inhibition rate in IT cell was larger than that of ET cell. I also found that inhibition of $I_{Na,P}$ by riluzole puff

application prevented persistent activity maintenance of ET cell. These results suggest possibility that the gap of $I_{Na,P}$ density contribute to different intrinsic excitability between ET and IT cell.

To investigate further on effect of intrinsic excitability modulation in specific cell group, I targeted cortico-striatal PN which is categorized as IT cell. PNs of the mPFC transmit glutamatergic input to medium spiny neurons of the direct and in direct pathway (dMSNs and iMSNs, respectively), and unbalanced activity of these neurons mediates reward-related behaviors induced by addictive drugs. Prelimbic (PL) input to MSNs in the nucleus accumbens core (NAcC) plays a key role in cocaine-induced early locomotor sensitization (LS). However, the adaptive plastic changes at PL-to-NAcC synapses underlying early LS remain unclear. Using transgenic mice and retrograde tracing, I identified NAcC-projecting PNs in the PL cortex based on the expression of dopamine receptor types. To examine cocaine-induced alterations in PL-to-NAcC synapses, I measured EPSC amplitudes evoked by opto-stimulation of PL afferents to MSNs. Riluzole was chosen to test the effects of PL excitability on cocaine-induced changes of PL-to-NAcC synapses. As a result, I found that NAcC-projecting PNs were segregated into D1R- and D2R-expressing PNs (D1-

and D2-PNs, respectively), and their excitability was opposingly regulated by respective dopamine agonists. Both D1- and D2-PNs exhibited balanced innervation of dMSNs and iMSNs in naïve animals. Repeated cocaine injections resulted in biased synaptic strength toward dMSNs through presynaptic mechanisms both in D1- and D2-PNs, although D2R activation reduced the D2-PN excitability. Under group 1 mGluRs co-activation, however, D2R activation enhanced the D2-PN excitability. The cocaine-induced rewiring accompanied LS, and both rewiring and LS were precluded by PL infusion of riluzole, which reduced the intrinsic excitability of PL neurons. These findings indicate that cocaine-induced rewiring of PL-to-NAcC synapses correlates well with early behavioral sensitization, and that rewiring and LS can be prevented by riluzole-induced reduction of excitability of PL neurons.

Keywords : Persistent Na^+ current, Medial prefrontal cortex, Prelimbic cortex, Nucleus accumbens core, Reward circuit, presynaptic dependent plasticity, cocaine sensitization

Student Number : 2014-22023

Contents

List of Figures

Chapter.1

Difference in electrophysiological properties and persistent Na^+ current contribution between extratelencephalic and intratelencephalic cells in prelimbic cortex

Introduction

The mammalian neocortex is composed of six layers. Pyramidal neurons (PNs) of each layer have different morphology and performs distinct functions (Jones and Peters 1990, Beltramo, D'Urso et al. 2013, Narayanan, Udvary et al. 2017, Radnikow and Feldmeyer 2018). Synaptic inputs from various region are processed as it passes through the layers, and processed signals are transmitted to other brain region via PNs in deep layer. To understand entire processing procedure of neocortex, it is therefore important to study in detail intrinsic properties of PNs in each layer, because, intrinsic properties of PN modify delivered input and affect firing generation which is responsible for transmitting signal.

The PNs of neocortex are broadly categorized into two groups depending on those of long-range projection target: intratelencephalic (IT) cells and extratelencephalic (ET) cells (Reiner, Jiao et al. 2003, Molnar and Cheung 2006, Gerfen, Economo et al. 2018, Saiki, Sakai et al. 2018). These two groups of excitatory neurons are distinguished by several properties. First, gene expression depends on the projection target (Gerfen, Paletzki

et al. 2013, Huang 2014, Harris and Shepherd 2015). These different gene expressions make it possible to reveal the role of neurons according to projection targets. For example, ET and IT cells were labeled using genetic strategy and they were shown to play distinct roles ET during working memory (Bae, Jeong et al. 2021). Second, ET and IT cells have different dendritic morphology. ET cell have thick tufted apical dendrite while IT cells have thin tufted apical dendrite(Morishima and Kawaguchi 2006). Finally, ET and IT cell have different intrinsic electrophysiological properties like input resistance and sag ratio (Sheets, Suter et al. 2011, Popescu, Le et al. 2017, Baker, Kalmbach et al. 2018). The existence of ET and IT cells in neocortex which have distinct properties implicates the necessity of target dependent cell type study.

The prefrontal cortex (PFC) which is one of the regions of the neocortex carries out “executive function” that captures information about external stimuli and compares them with past memories to select correct behavior (Shimamura 2000). The compared outcomes, which are processed in the prefrontal cortex, have different encoding contents depending on where it is headed. For example, projection to basolateral amygdala is responsible for

stress-induced anxiety (Liu, Zhang et al. 2020), projections to dorsal striatum and thalamus are involved in cognitive function (Schmitt, Wimmer et al. 2017, Terra, Bruinsma et al. 2020) and projection to nucleus accumbens underlies reward related behavior (Tzschentke 2000, Gill, Castaneda et al. 2010). The PNs of PFC are also categorized into ET and IT cells depending on projection target like other neocortical regions, and they are known to have distinct electrophysiological properties (Gee, Ellwood et al. 2012, Anastasiades, Marlin et al. 2018). However, it is not well understood how the differences in electrical properties between ET and IT cells are related with their different functions.

Intrinsic property which is determined by individual conductance modifies synaptic input and modulates excitability of the PNs. ET and IT cells in the PFC exhibit distinct electrophysiological properties, not only subthreshold properties like resonance and sagging which are dependent on density of hyperpolarization-activated cyclic nucleotide gated channel (HCN channel), but also suprathreshold properties like firing frequency and threshold (Dembrow, Chitwood et al. 2010). The intrinsic properties of PNs in the PFC are altered by several neuromodulators like norepinephrine, acetylcholine and serotonin which are transmitted from diverse

region (Avesar and Gulledge 2012, Kalmbach, Chitwood et al. 2013, Zhang, Cordeiro Matos et al. 2013, Cools and Arnsten 2022). Especially, persistent activity consisting of repetitive firing which are highly correlated with working memory capturing external information is sensitive to neuromodulators (Curtis and D'Esposito 2003). However, downstream mechanism of maintenance of this repetitive firing phenomenon is unclear.

Here, I report difference of intrinsic properties between ET and IT cells in PFC using retrograde tracing and electrophysiology. I elucidate that persistent Na^+ current ($I_{Na,P}$) density which performs critical role in sustaining repetitive firing is larger in ET cell than in IT cell, and group1 metabotropic glutamate receptor (mGluR) agonist induces persistent activity more sensitively in ET cell. Furthermore, I found that blocking of the $I_{Na,P}$ prevented group 1 mGluR agonist-induced persistent activity of ET cell. Altogether, I suggest that cell type specific contribution of $I_{Na,P}$ differently modulates intrinsic excitability of the PNs in the PFC.

Result

Intrinsic properties of ET and IT cell in prelimbic cortex

To discriminate ET and IT cell, I injected Retrobead Red, a retrograde tracer, to mPFC for labeling contralateral prelimbic PNs (Figure 1A). These neurons which have cortico-cortical connection are classified as IT cell category (Anastasiades, Marlin et al. 2018). Interestingly, although retrograde tracer was injected to entire contralateral mPFC, labeled neurons were mostly found in the prelimbic cortex, while rarely found in the infralimbic cortex (Figure 1B). This result implicates exquisite segmentation of projection. To obtain electrophysiological properties of ET and IT cell, I conducted whole-cell patch clamp at layer 5 of prelimbic cortex (Figure 1C). Among unlabeled neurons, I selected neurons with thisk apical tuft as ET cells.(Gee, Ellwood et al. 2012). The resting membrane potential of ET and IT cell was not different significantly (Figure 1D), but, the hyperpolarizing current pulse injection showed different electrophysiological properties between ET and IT cell (Figure 1E). Input resistance of IT cell was prominently larger than that of ET cell, similarly with study of

Kalmbach et al (Kalmbach, Chitwood et al. 2013) (Figure 1F). The sag ratio of ET cell was larger than that of IT cell sag ratio (Figure 1G), because ET cell has high density of hyperpolarization-activated cyclic nucleotide gated channel (Dembrow, Chitwood et al. 2010). These results suggest that excitability of PNs in prelimbic cortex might be different according to their projection target.

To compare the excitability between ET and IT cell, I measured the number of spikes evoked by step depolarizing current injections from a −65 mV membrane potential (Figure 1H, I). Although the two-way repeated-measure ANOVA analysis (Cell type x Injection current) did not showed significant difference between two group in F-I curve, post-hoc test revealed significant difference in 100 pA and 150 pA current injections (Figure 2J). The action potentials evoked by these low current injections showed a similar frequency with spikes of ET and IT cell recorded in in vivo state (mostly < 10 Hz)(Bae, Jeong et al. 2021). This means that IT cell has a larger intrinsic excitability than ET cell in physiological conditions. The high input resistance of IT cell (Figure 1A) might result in difference of intrinsic excitability.

The persistent activity, maintenance of repetitive firing followed by depolarization pulses, is another parameter of intrinsic

excitability (Le Bon-Jego and Yuste 2007). This firing can be triggered by mGluR activation induced afterdepolarization (ADP) which is a prolonged response to a preceding depolarizing stimulus (Sidiropoulou, Lu et al. 2009). To examine the persistent activity generating capability of ET and IT cell, I elicited delayed ADP response to depolarizing current injection (100 pA) from a holding potential of −60 mV in the presence of DHPG, group 1 metabotropic glutamate receptor agonist (Figure 2A). I found that the persistent activity occurred at a high rate in ET cell than in IT cell (Figure 2B). Despite of high input resistance in IT cells, DHPG-induced persistent activity was generated more prominently in ET cells. These results imply that an existence of another mechanism underlying delayed ADP dependent persistent activity generation, compared to depolarization-induced repetitive firing in control condition.

Different expression of $I_{Na,P}$ between ET and IT cells and effects of riluzole

The $I_{Na,P}$ is a non-inactivating component of the sodium current which is important for repetitive firing (Urbani and Belluzzi 2000), so I explored contribution of $I_{Na,P}$ on persistent activity of ET and IT

cell to investigate firing properties in depth. First, I recorded $I_{Na,P}$ responding to a slow voltage ramp pulse in ET and IT cell (Figure 3A, B), and found significant difference of $I_{Na,P}$ density between ET and IT cell (Figure 3C). To confirm this hypothesis, I conducted puff application of riluzole, a blocker for $I_{Na,P,}$ during repetitive firing (Figure 3E), and actually, riluzole puff to soma of ET cell decreased firing frequency or terminated firing (Figure 3F). These data suggest that $I_{Na,P}$ plays as a key role in persistent activity.

To further test contribution of $I_{Na,P}$ on excitability, I modulated $I_{Na,P}$ by riluzole bath application. I used 5 μM riluzole which was sufficient to reduce the $I_{Na,P}$ by more than 50 % in both ET and IT cell (Figure 3D), but had negligible non-specific effects on K^+- or Ca^{2+} currents (Bellingham 2011). Decreased $I_{Na,P}$ by riluzole significantly reduced number of spikes in both ET and IT cell (Figure 4A), but riluzole effect was larger in IT cell than in ET cell (Figure 4B). I speculated that this result came from the difference in remaining $I_{Na,P}$ amplitude of ET and IT cell.

Discussion

In the present study, I examined electrophysiological properties and contribution of $I_{Na,P}$ on intrinsic excitability in ET and IT cell in prelimbic cortex. I identified ET and IT cell based on morphological property and retrograde tracing labeling. These cells had similar resting membrane potential, but, they had different subthreshold intrinsic properties (Figure 1). ET and IT cell also showed different intrinsic excitability. The firing frequency in response to step depolarizing current injection in IT cell was greater than in ET cell, while ET cell showed more strong propensity of occurrence of persistent activity triggered by delayed ADP than IT cell (Figure 2). Lastly, I compared $I_{Na,P}$ amplitude and $I_{Na,P}$ blocking effect between ET and IT cell for exploring $I_{Na,P}$ contribution to intrinsic excitability (Figure 3, 4). The $I_{Na,P}$ amplitude in ET cell was larger than in IT cell. I also found that blocking of $I_{Na,P}$ by riluzole prevented mGluR-induced persistent activity in ET cell, while IT cell was more sensitive to riluzole than ET cell in reducing depolarization-induced firing. My results suggest that gap of $I_{Na,P}$ density might render distinct intrinsic excitability to ET and IT cell.

Previous studies have shown that $I_{Na,P}$ plays a key role in repetitive firing (Siniscalchi, Bonci et al. 1997, Urbani and Belluzzi 2000, Pieri, Carunchio et al. 2009, Bellingham 2011). First, $I_{Na,P}$ which is activated in subthreshold potential provides depolarization current during inter spike interval (Crill 1996). Second, density of $I_{Na,P}$ contributes to action potential threshold (Lampl, Schwindt et al. 1998, Katz, Stoler et al. 2018). These factors increase repetitive firing, so, in this point of view, I hypothesized that different $I_{Na,P}$ density could be a one of factor for difference of intrinsic excitability of ET and IT cell in the prelimbic cortex. Actually, I found that ET cell had larger $I_{Na,P}$ amplitude than ET cell. Despite of lower $I_{Na,P}$ density, IT cell showed higher firing frequency response to sustained current injection than ET cell in control condition (Figure 1J). I speculate that this result comes from difference in input resistance that almost twice (Figure 1G). To figure out the contribution of $I_{Na,P}$ on intrinsic excitability, I blocked $I_{Na,P}$ using riluzole and I found that decrease in number of spikes by riluzole was more prominent in IT cell than in ET cell. These results suggest that repetitive firing of cells with low $I_{Na,P}$ density were more vulnerable to $I_{Na,P}$ reduction.

It has been known that activation of Gq protein receptors such as

muscarinic or metabotropic glutamate receptor elicits delayed ADP triggering persistent activity (Zhang, Cordeiro Matos et al. 2013). Here, I elicited persistent activity using DHPG, group1 mGluR agonist, and found that persistent activity occurred with higher rate in ET cells than IT cells (Figure 2B), despite it is known that amplitude of dADP induced by DHPG is similar in ET cells and IT cells (Kalmbach, Chitwood et al. 2013). Based on the previous studies which showed that the threshold of IT cell is more depolarized than those of ET cell and that reduced $I_{Na,P}$ depolarizes threshold (Dembrow, Chitwood et al. 2010, Katz, Stoler et al. 2018), it can be speculated that the result of figure 2B might be due to the different density of $I_{Na,P}$. Possibly, ADP is sufficient to generate action potential in ET cells that have low threshold due to large $I_{Na,P}$. Furthermore, the result that riluzole prevented repetitive firing during persistent activity suggests that $I_{Na,P}$ is also important to maintain persistent activity. Altogether, $I_{Na,P}$ could differently contribute to excitability of PNs depends on projection target, and it means that the role of PFC determined by direction of transmission might be affected by $I_{Na,P.}$

In summary, ET and IT cells in the PFC have different intrinsic properties, and different density of $I_{Na,P}$ contributes to these distinct

intrinsic excitability.

Materials and methods

Animals and ethical approval

I used wild-type C57BL/6 male mice for experiments (purchased from OrientBio) All animal studies and experimental protocols were approved by the Institutional Animal Care and Use Committee (IACUC, approval No. SNU-190716-6) at Seoul National University. The animals were maintained at standard environmental conditions (25 ± 2 ° C; 12/12 h dark/light cycle) and were housed under veterinary supervision at the Institute for Experimental Animals, Seoul National University College of Medicine.

Surgery

For retrograde tracing, I injected 1 μl of Red Retrobeads (Lumafluor) to medial prefrontal cortex of 6-week-ild mice. Stereotaxic coordinate was AP +1.65, ML +0.35 and DV -2.2 mm. A syringe pump (WPI, MICRO2T) was used for infusion at 100 nL/min and injection needle was withdrawn 10 min after the end of the infusion. Animals were anesthetized with 5% isoflurane for the duration of stereotaxic surgery.

Slice preparation

Coronal mPFC slices were obtained from P56−70 mice. After mice anaesthetized by inhalation with 5% isoflurane, they were decapitated and the brain quickly removed and chilled in an ice−cold high magnesium cutting solution containing the following (in mM): 110 choline chloride, 25 $NaHCO_3$, 20 Glucose, 2.5 KCl, 1.25 NaH_2PO_4, 1 Sodium pyruvate, 0.5 $CaCl_2$, 7 $MgCl_2$, 0.57 Ascorbate, with pH adjusted to 7.4 by saturating with carbogen (95% O2, 5% CO2), and with osmolality of approximately 300 mOsm/L. The isolated brain was glued onto the stage of a vibrating blade microtome (Leica VT1200) and 300 μm−thick slices were cut. The slices were incubated at 36 ° C for 30 min in the artificial cerebrospinal fluid (aCSF) containing the following (in mM): 125 NaCl, 25 $NaHCO_3$, 20 Glucose, 2.5 KCl, 1.25 NaH_2PO_4, 1 Sodium pyruvate, 2 $CaCl_2$, 1 $MgCl_2$, 0.57 Ascorbate, bubbled with 95% O_2 and 5% CO_2., and thereafter maintained at room temperature.

Whole−cell patch clamp

Whole−cell voltage− or current−clamp recordings were performed at 32 ± 1° C and the rate of aCSF perfusion was maintained at 1−1.5 ml/min. The recordings were made in somata with EPC−10

amplifier (HEKA Electronik) at a sampling rate of 20−25 kHz. Patch pipettes (3-4 MΩ) for recordings were filled with internal solution containing the following (in mM): 125 Potassium gluconate, 10 KCl, 4 NaCl, 20 HEPES, 1 $MgCl_2$, 4 MgATP, 0.3 NaGTP, 0.1 EGTA (pH 7.3 with KOH). For persistent sodium current experiments, pipettes filled with a Cs−based internal (in mM): 120 Cs−methanesulfonate, 10 CsCl, 10 HEPES, 1 $MgCl_2$, 3 MgATP, 0.4 NaGTP, 5 Na_2 phosphocreatine, 0.1 EGTA, 5 QX−314, 10 tetraethylammonium chloride (TEA) (pH 7.3 with CsOH).

Recordings were made with 50 μM DL−APV (APV) to block NMDARs (not used in AMPA/NMDA current ratio), 100 μM picrotoxin to block $GABA_A$ and 1 μM CGP52432 to block $GABA_B$ bath application. In persistent sodium currents experiments, 20 mM TEA and 0.2 mM $CdCl_2$ were added to aCSF. I monitored series resistance throughout experiments, and excluded recordings with series resistance >25 MΩ from data analysis. Series resistance was not compensated. All electrophysiology data were recorded exclusively in layer5 of PL in right hemisphere.

The input resistance (R_{in}) and sag ratios were calculated from 500 ms and −50 pA current injections. R_{in} was calculated from the steady−state voltage during the current injection. The voltage sag

was defined as the ratio of the maximum to steady-state voltage ($V_{Min}-V_{Baseline}$) / ($V_{Steady}-V_{Baseline}$), where V_{Min} is the minimum peak during the first 25 ms, V_{Steady} is the average of the last 25 ms, and $V_{Baseline}$ is the average of the 25 ms preceding the current injection. To elicit persistent activity, 20 μM DHPG (or DHPG and quinpirole together) was bath-applied for at least 20 min. Persistent activity was defined as the maintenance of firing that occurred for 1 min after the 100 pA, 1 s current injection at a membrane potential of -60 mV. If firings did not occur within 5 s after the current injection, or if fewer than five firings occurred, I classified the group as a non-burst group. The point at which the firing stopped for more than 5 s was defined as the termination time. Persistent sodium currents were recorded using a slowly increasing voltage ramp pulse (10 mV/s) from a holding potential of -60 mV to 0 mV in a voltage-clamp configuration. To obtain only tetrodotoxin-sensitive currents, I recorded 1 μM tetrodotoxin bath-applied traces to subtract values from the original trace.

Data Analysis

All data were presented as mean ± standard error of the mean (SEM). Statistical analysis was performed using IgorPro (version

7.08, WaveMetrics) and SPSS (version 26, IBM). Unless otherwise stated, nonparametric Mann-Whitney U test was used to compare non-paired groups, and paired sample t test was used to compare paired groups, respectively. F-I curve was assessed using Greenhouse-Geisser corrected two-way repeated measures ANOVA followed by Bonferroni's post hoc tests. P-values of < 0.05 were considered statistically significant.

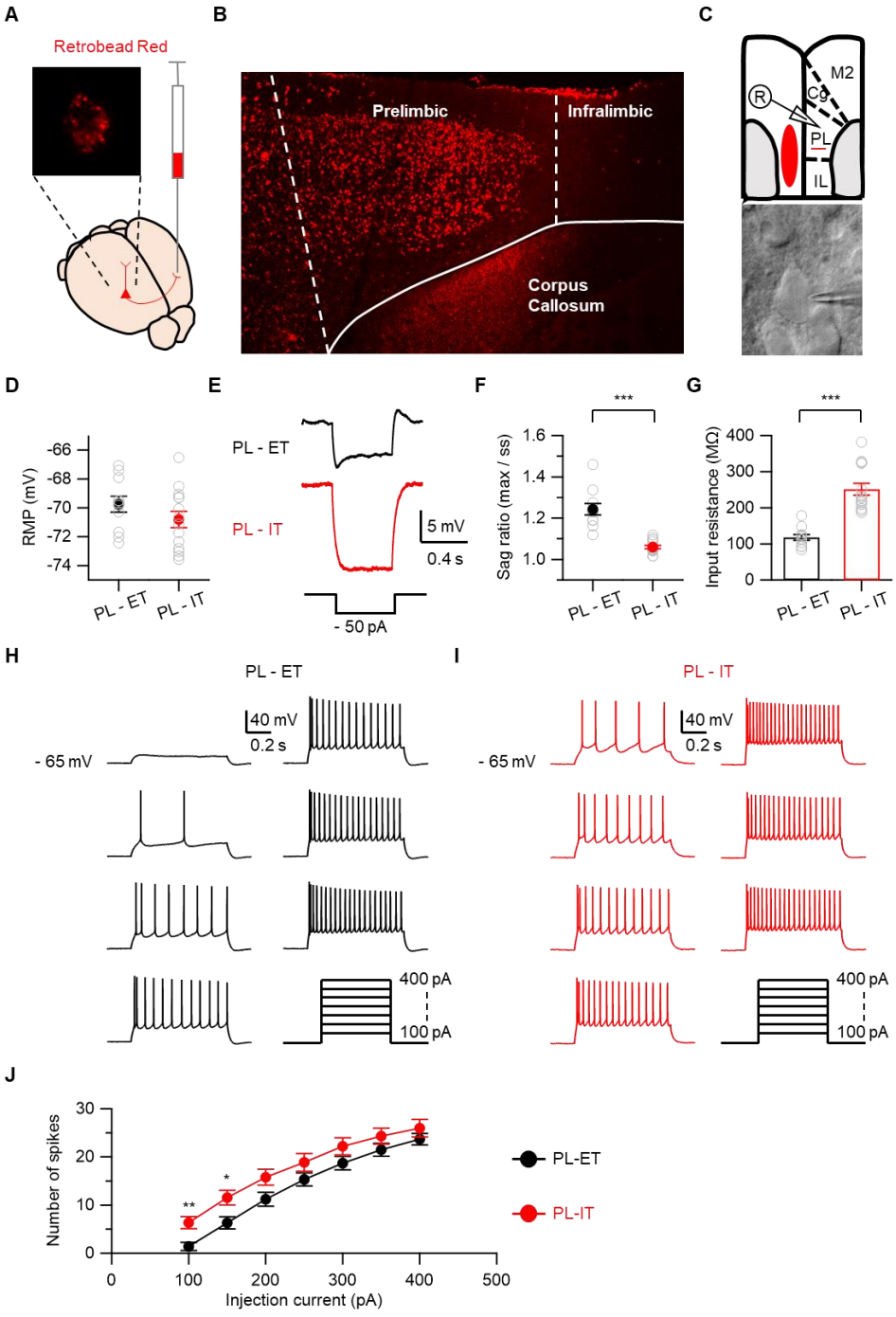
A
Retrobead Red
B
Prelimbic
Infralimbic
Corpus
Callosum
C
M2
Cg
R
PL
IL
D
RMP (mV)
-66
-68
-70
-72
-74
PL - ET
PL - IT
E
PL - ET
PL - IT
5 mV
0.4 s
- 50 pA
F
***
Sag ratio (max / ss)
1.6
1.4
1.2
1.0
PL - ET
PL - IT
G
***
Input resistance (MΩ)
400
300
200
100
0
PL - ET
PL - IT
H
PL - ET
40 mV
0.2 s
- 65 mV
400 pA
100 pA
I
PL - IT
40 mV
0.2 s
- 65 mV
400 pA
100 pA
J
Number of spikes
30
20
10
0
0
100
200
300
400
500
Injection current (pA)
**
*
PL-ET
PL-IT

Figure 1. Intrinsic properties of ET and IT cell in prelimbic cortex

(A) Schematic of Retrobead Red injection into the contralateral PFC and labeled single ET cell. (B) Confocal images of labeled IT cells in a PFC. (C) *Upper*, schematic for the recording electrophysiological data. *Lower*, DIC images showing somatic patch-clamp recording. (D) Resting membrane potentials of ET (black) and IT (red) cells (PL-ET, -69.76 ± 0.54 mV, n = 11; PL-IT, -70.81 ± 0.57 mV, n = 14, p = 0.25). (E) Representative traces of a PL-ET and PL-IT in response to -50 pA hyperpolarizing current. (F) Summary for input resistance and sag ratio. *Left*, mean input resistance (PL-ET, 117.7 ± 8.12 MΩ, n = 11; PL-IT, 251.56 ± 16.51 mV, n = 14, p < 0.001), *Right*, mean sag ratio (PL-ET, 1.24 ± 0.03, n = 11; PL-IT, 1.06 ± 0.01 MΩ, n = 14, p < 0.001). (H-I) Representative voltage responses to step depolarizing current injection of ET cell (H) and IT cell (I) (J) Number of spikes evoked by depolarizing steps of increasing current of ET and IT cell. (PL-ET vs PL-IT, Cell type x Injection current: $F_{(2, 12.29)}$ = 1.74, p=0.198; post hoc T-test: 100 pA, p < 0.01; 150 pA, p < 0.05; 200pA, p = 0.052; 250 pA, p= 0.132; 300 pA, p = 0.133; 350 pA, p = 0.203; 400 pA, p = 0.292, two-way repeated measure ANOVA and Bonferroni's post hoc test). Data are

shown as mean ± SEM. $^{***}p < 0.001$

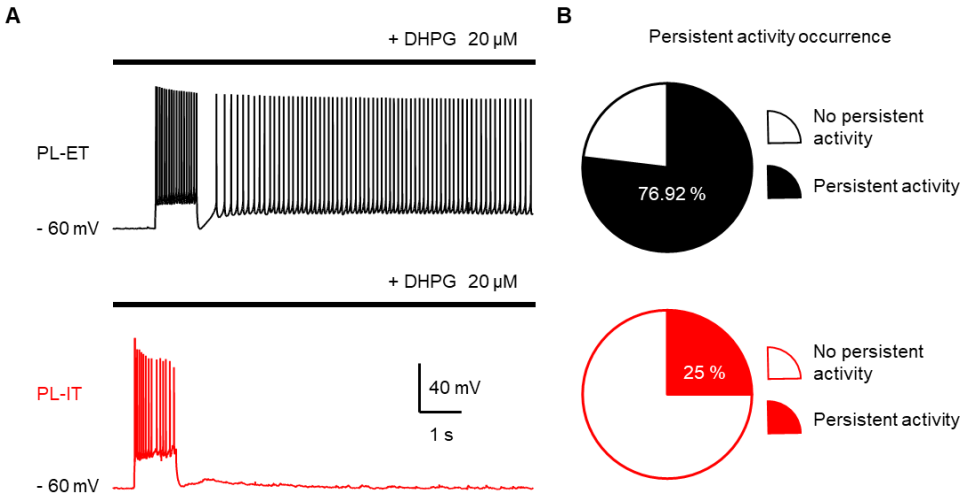
A
+ DHPG 20 µM
PL-ET
- 60 mV
+ DHPG 20 µM
PL-IT
- 60 mV
40 mV
1 s
B
Persistent activity occurrence
76.92 %
No persistent activity
Persistent activity
25 %
No persistent activity
Persistent activity

Figure 2. DHPG-induced persistent activity generation is more prominent in ET cell than IT cell

(A) Representative traces of 20 μM DHPG-induced persistent activity in ET cell (*upper*) and IT cell (*lower*). **(B)** Proportions of DHPG-induced persistent activity occurred cell in ET cell group (*upper*, occurred n = 10 / total n = 13) and IT cell group (*lower*, occurred n = 3 / total n = 12). Data are shown as mean ± SEM. $^{*}p < 0.05$, $^{**}p < 0.01$.

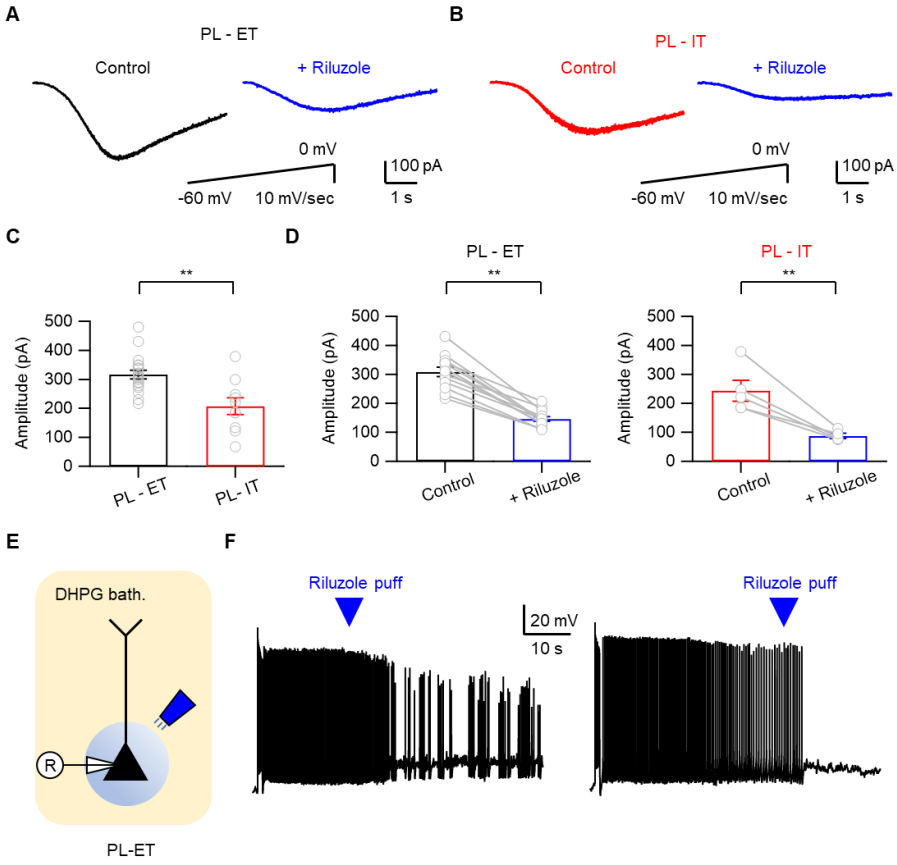
A
PL - ET
Control
+ Riluzole
0 mV
-60 mV
10 mV/sec
100 pA
1 s
B
PL - IT
Control
+ Riluzole
0 mV
-60 mV
10 mV/sec
100 pA
1 s
C
**
Amplitude (pA)
500
400
300
200
100
0
PL - ET
PL- IT
D
PL - ET
**
Amplitude (pA)
Control
+ Riluzole
PL - IT
**
Amplitude (pA)
Control
+ Riluzole
E
DHPG bath.
R
PL-ET
F
Riluzole puff
20 mV
10 s
Riluzole puff

Figure 3. Large $I_{Na,P}$ in ET cell contributes to persistent activity

(A–B) Representative traces of $I_{Na,P}$ evoked by applying a slow voltage ramp pulse befor (black) and after (blue) bath application of 5 μM riluzole in ET cell (A) and IT cell (B). **(C)** Summary of the $I_{Na,P}$ amplitude in ET cell and IT cell (PL–ET, 316.83 ± 14.53 pA, n = 19; PL–IT, 207.46 ± 28.62 pA, n = 19, $p < 0.01$). **(D)** Summary of the $I_{Na,P}$ amplitude before and after 5 μM riluzole in ET cell (left; control, 308.53 ± 16.22 pA; riluzole, 145.82 ± 8.2 pA, n = 13, $p < 0.01$) and IT cell (right; control, 243.23 ± 35.83 pA; riluzole, 87.18 ± 9.0 pA, n = 5, $p < 0.01$). **(E)** Experimental configuration showing the whole–cell patch clamp recording with puff application of 25 μM riluzole in PL–ET cell. **(F)** Representative traces showing prevention of persistent activity by 25 μM riluzole puff application at 20 sec (*left*) and 40 sec (*right*) after end of the depolarizing current injection.

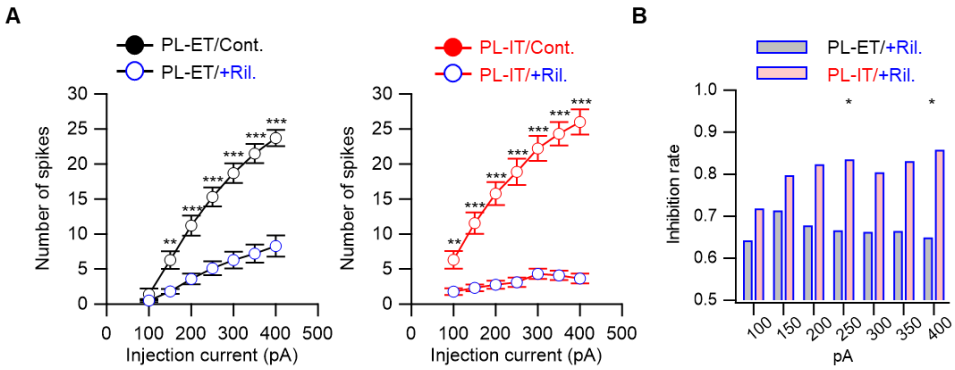
A
PL-ET/Cont.
PL-ET/+Ril.
Number of spikes
Injection current (pA)
PL-IT/Cont.
PL-IT/+Ril.
Number of spikes
Injection current (pA)
B
PL-ET/+Ril.
PL-IT/+Ril.
Inhibition rate
pA

Figure 4. Different density of $I_{Na,P}$ causes different sensitivity to riluzole for repetitive firing

(A) Number of spikes evoked by depolarizing step current injections in ET cell (*Left*) and IT cell (*Right*), before and after 5 μM riluzole (blue) bath application. (PL−ET, control vs riluzole, Treatment x Injection current: $F_{(1.9, 22.98)} = 32.46$, $p < 0.001$; post hoc T−test: 100 pA, $p = 0.31$; 150 pA, $p < 0.01$; 200pA, $p < 0.001$; 250 pA, $p < 0.001$; 300 pA, $p < 0.001$; 350 pA, $p < 0.001$; 400 pA, $p < 0.001$, $n = 10$; PL−IT, control vs riluzole, Treatment x Injection current: $F_{(1.4, 22.52)} = 25.16$, $p < 0.001$; post hoc T−test: 100 pA, $p < 0.01$; 150 pA, $p < 0.001$; 200pA, $p < 0.001$; 250 pA, $p < 0.001$; 300 pA, $p < 0.001$; 350 pA, $p < 0.001$; 400 pA, $p < 0.001$, $n = 9$, two−way repeated measure ANOVA and Bonferroni's post hoc test). **(B)** Summary for inhibition rate calculated in Figure 3G. Data are shown as mean ± SEM. $^{*}p < 0.05$, $^{**}p < 0.01$, $^{***}p < 0.001$.

Chapter.2

Rewiring of prelimbic inputs to the nucleus accumbens core underlies cocaine-induced behavioral sensitization

Introduction

Addictive drugs elevate dopamine (DA) levels within mesocorticolimbic reward circuits, leading to pathological reward-related behaviors (Hyman, Malenka et al. 2006). Repeated exposure to addictive drugs induces progressive enhancement of motor activity, known as behavioral sensitization. As a signaling hub, the nucleus accumbens (NAc) integrates glutamatergic inputs (Tzschentke and Schmidt 2003) and modulates behavioral outcomes by providing prioritizing signals to downstream basal ganglia. NAc is a part of the basal ganglia-thalamocortical circuitry. Medium spiny neurons (MSNs), the principal cells of NAc, are composed of two types depending on their projection targets. They project to the ventral tegmental area (VTA)/substantia nigra pars reticulata (SNr) or ventral pallidum (VP), which constitute direct and indirect pathways, respectively (Heimer, Zahm et al. 1991, Smith, Bevan et al. 1998, Sesack and Grace 2010, Hikida, Yawata et al. 2013). These two pathways exert bidirectional effects on motor outcomes and reward-related behaviors by modulating thalamic activity (Hikida, Kimura et al. 2010, Kravitz, Tye et al. 2012, Hikida, Yawata et al. 2013). In the present study, I refer to MSNs projecting to the VTA or VP as MSNs belonging to either direct or

indirect pathways (denoted as dMSNs and iMSNs), respectively.

Previous studies have shown that an increase in the glutamatergic synaptic transmission in the NAc core (NAcC), but not in the shell, underlies cocaine-induced early behavioral responses such as locomotor sensitization (LS) and drug seeking (Pierce, Reeder et al. 1998, Di Ciano and Everitt 2001). Cocaine-induced LS can be elevated by high frequency stimulation of the direct pathway and correlates with the activity of D1 receptor (D1R)-expressing MSNs in the NAc (D1-MSNs) (Bocklisch, Pascoli et al. 2013, van Zessen, Li et al. 2021). Consistently, blockade of the direct pathway, but not the indirect pathway, prevented cocaine-induced LS, suggesting that cocaine induces neural maladaptation such that the direct pathway plays a predominant role in cocaine sensitization (Hikida, Kimura et al. 2010).

D1-MSNs and D2-MSNs largely comprise the direct and indirect pathways of the ventral striatum, respectively (Durieux, Bearzatto et al. 2009, Hikida, Kimura et al. 2010, Bock, Shin et al. 2013, Hikida, Yawata et al. 2013). It was recently shown, however, that a portion of D1-MSNs projects also to the VP (Kupchik, Brown et al. 2015), and encodes aversive memory (Liu, Le et al. 2022). Moreover, excitatory inputs from the amygdala to D1-MSNs undergo distinct synaptic plasticity depending on their projection

targets, the VTA or the VP (Baimel, McGarry et al. 2019). These previous findings prompt further investigation of pathway-dependent connectivity changes after cocaine exposure.

Glutamatergic inputs to the NAcC play a key role in early emergence of cocaine-induced LS (Kalivas, Lalumiere et al. 2009). In contrast, the LS expressed after a prolonged withdrawal of cocaine correlated well with potentiation of excitatory synaptic inputs to D1-MSNs of the NAc shell (Pascoli, Turiault et al. 2012). Moreover, while medial prefrontal cortex (mPFC) inputs have been implicated in cocaine-induced early development of LS (Pierce, Reeder et al. 1998), the relative strength of mPFC inputs to D1- and D2-MSNs of the NAc shell remained unbiased in cocaine-treated mice after short-term withdrawal (MacAskill, Cassel et al. 2014). These studies imply that distinct synaptic mechanisms underlie LS expression during the early and late cocaine withdrawal periods. The mPFC is a major glutamatergic input source to the NAcC (Brog, Salyapongse et al. 1993), but the plastic changes at mPFC-to-NAcC connections underlying early phase addictive behaviors remain poorly understood.

The mPFC, which belongs to the mesocorticolimbic circuitry, receives dopaminergic input from the VTA. In layer 5 (L5) of the mPFC, pyramidal neurons (PNs) are largely segregated into two

populations: PNs expressing D1R and D2R (denoted as D1−PNs and D2−PNs, respectively). It is known that D1−PNs and D2−PNs correspond to L5 PNs projecting to the extra− and intra−telencephalon (IT and ET cells), respectively, based on their distinct intrinsic properties (Gee, Ellwood et al. 2012, Seong and Carter 2012). A recent study, however, showed that some D1R−lacking PNs have the electrophysiological properties of IT cells (Anastasiades, Marlin et al. 2018). As the NAc is heavily innervated by IT cells, it is plausible that D2−PNs may innervate the NAc. Given that the activation of D1− or D2 receptors (D1R or D2R) opposingly modulates the excitability of pyramidal neurons (PNs) in mPFC (Yang and Seamans 1996, Gulledge and Jaffe 1998, Wang and O'Donnell 2001, Dong, Nasif et al. 2005, Anastasiades, Marlin et al. 2018). , it needs to be addressed whether D1− or D2−PNs innervate distinct MSN populations in the NAc and how the connections of D1 and D2−PNs in the mPFC to the NAcC are differentially modulated by repeated cocaine exposure.

I explored whether D1− and D2−PNs in the mPFC would display different synaptic strength to MSNs of the NAcC depending on their projection targets and how their excitability could regulate cocaine−induced behavioral changes. Here I show that 1) not only D1− but also D2−PNs in the prelimbic (PL) cortex equally

innervate the MSNs of the direct and indirect pathways; 2) repeated cocaine exposure biases the output of both D1− and D2−PNs of the PL toward MSNs of the direct pathway; and 3) riluzole infusion into the PL cortex prevents this cocaine−induced biasing of PL−NAcC connections and LS in parallel.

Results

Both D1R- and D2R-expressing prelimbic neurons innervate NAcC

To explore the effects of DA on the PL cortex, I investigated which receptor was expressed in individual PL NAcC-projecting PNs. I injected Retrobeads into the NAcC to label NAcC-projecting neurons in the PL cortex and characterized the effects of D1 and D2 agonists on the excitability of the retrobead-labeled NAcC-projecting PNs in layer V of the PL cortex (Figure 1A). To this end, I bath-applied either a D1 or D2 agonist (10 μM SKF 81297 or 10 μM quinpirole, respectively) and quantified the excitability changes as the difference in the number of spikes evoked by somatic injection of 100 pA before and after agonist application (⊿AP) (Figure 1B-C). Because of prolonged effects of DA agonists on the excitability (Chen, Bohanick et al. 2007), I could not test both agonists in the same cell. From the bimodal distribution of ⊿AP (Figure 1B-C), NAcC-projecting PNs could be divided into responders and non-responders to D1 or D2 agonists, suggesting that a subset of NAcC projecting PNs express D1R or D2R (D1 responder, 10/25 cells; D2 responder, 14/27 cells).

To corroborate the expression of D1R or D2R in NAcC-projecting PNs, I injected AAV encoding double floxed EYFP into the PL cortex of Drd1- or Drd2-cre mice, and then injected CTB-Alexa 647 into the NAcC two weeks later. Some CTB(+) PNs expressed EYFP in Drd1- and Drd2-cre mice, indicating that both D1R- and D2R-expressing PNs (denoted as D1-PN and D2-PN, respectively) innervate NAcC (Figure 1D-E and 2-3). The voltage responses to -50 pA indicated that D1- and D2-PNs did not differ in sag ratio or input resistance (R_{in}) (Fig. 1F). This result is not consistent with the previous observation that the sag ratio of D2-PN was larger than that of D1-PN (Gee, Ellwood et al. 2012, Seong and Carter 2012), probably because I focused on PL NAcC-projecting L5 PNs in my analysis, whereas PL L5 PNs in general were previously tested. The low sag ratio and high R_{in} of NAcC-projecting PL neurons are reminiscent of the well-established sub-threshold electrical properties of L5 IT cells (Sheets, Suter et al. 2011, Baker, Kalmbach et al. 2018). I also compared the number of spikes evoked by the somatic injection of +100 pA (Figure 1G). The number of evoked spikes did not differ between the D1- and D2-PNs. Finally, I examined the AP response changes (ΔAP) induced by bath application of D1 or D2 agonist in D1- or D2-PNs (Figure 1H,1I). As expected, D1-PNs and D2-PNs responded to

their respective agonists. In 5 out of 34 PNs, ⊿AP induced by a counterpart DA agonist were in the 2 S.D. range of ⊿AP of the other PN group, suggesting a possible co-expression of D1R and D2R in a small proportion of PN (Figure 4). Little effect of DA agonists on the AP threshold of PL neurons argues against the possibility that the DA agonist effects are mediated by changes in spontaneous recurrent synaptic inputs (Figure S4). Altogether, my data indicate that a subset of PL NAcC-projecting PNs express either D1R or D2R, which have similar intrinsic properties and largely constitute two distinct populations.

Connectivity between the PL and NAcC regions

The final motor outcomes resulting from DA-mediated differential excitability regulation of D1- and D2-PNs may depend on the relative synaptic strength of D1- and D2-PNs to dMSNs and iMSNs. To selectively stimulate the axons of D1 or D2-PNs innervating dMSNs and iMSNs, I injected AAV encoding double floxed ChR2 into the PL cortex of Drd1- or Drd2-cre mice and then injected CTB-Alexa 555 and CTB-Alexa 647 into the VTA and VP two weeks later (Figure 5A, 6). The dMSNs and iMSNs displayed neither topographic localization within NAcC (Figure 5B), nor a difference in intrinsic properties (Figure 7). The EPSCs

optically elicited from MSNs were completely abolished by bath applied 1 μM TTX, a sodium channel blocker, and subsequently restored by 0.1 mM 4-AP, a potassium channel blocker (Figure 8), indicating the monosynaptic projections from PL neurons to NAcC MSNs.

To investigate the relative projections of PL neurons to dMSNs and iMSNs in the NAcC, I recorded the EPSCs evoked by opto-stimulation of PL afferents in a pair of neighboring dMSNs and iMSNs in the same slice (denoted as dMSN-EPSCs and iMSN-EPSCs, respectively; Figure 5C) (Baimel, McGarry et al. 2019, Cummings and Clem 2020). The EPSC amplitude pairs were plotted on amplitude planes of iMSN-EPSCs *vs.* dMSN-EPSCs evoked by optical stimulation of afferents from D1- or D2-PNs (Figure 5D-E). Following opto-stimulation of either of D1- or D2-PN afferents, the dMSN-EPSCs were largely proportional to the iMSN-EPSCs. With regard to the number of pairs on either side of the identity line on the plot, D1-PN inputs were slightly biased to dMSNs (the number of pairs such that dMSN-EPSCs > iMSN-EPSCs, n = 13; dMSN < iMSN, n=8) (Figure 5D), whereas D2-PN inputs were to iMSNs (dMSN > iMSN, n = 7; dMSN < iMSN, n = 9) (Figure 5E). However, the ratios of iMSN- /dMSN-EPSC amplitudes measured in each pair did not differ between the D1-

and D2-PN afferents (Figure 5F). Furthermore, for both afferents from D1 and D2-PNs, neither the amplitudes nor paired pulse ratios (PPRs) differed between the dMSN- and iMSN-EPSCs (Figure 5G-H). These results indicate that innervation of dMSNs and iMSNs by PL neurons is largely balanced for both prelimbic afferent types.

Cocaine administration biases projections from the PL cortex toward dMSNs of NAcC through presynaptic mechanisms

Next, I explored whether addictive drugs, such as cocaine, have any effect on the balanced projections of PL neurons to NAcC. I intra-peritoneally (i.p.) injected mice with either saline or 20 mg/kg cocaine for five consecutive days. The next day, I examined *ex vivo* whether cocaine induced any changes in PL projections to the NAcC (Figure 9A). Representative EPSC traces measured in dMSN (blue) and iMSN (red) pairs are overlaid in Figure 9B following opto-stimulation of D1- or D2-PNs in saline- or cocaine treated mice. Remarkably, after repeated cocaine exposure, the amplitudes of the dMSN-EPSCs were larger than those of the iMSN-EPSCs in most pairs regardless of their presynaptic afferent types (Figure 9C-D, 9F-G). The iMSN-EPSC/dMSN-EPSC ratios were significantly lower in cocaine-treated mice than in saline-

treated mice for both afferent types (Figure 9E, 9H). For both D1 and D2 afferents, the amplitudes of the dMSN-EPSCs were not different from those of the iMSN-EPSCs in saline-treated mice (Figure 9I-J). After cocaine administration, the dMSN-EPSC amplitudes were significantly larger than the iMSN-EPSC amplitudes following D2 afferent stimulation ($p < 0.05$), whereas the former was only marginally larger than the latter upon D1 afferent stimulation ($p = 0.055$) (Figure 9I-J).

To examine the attributes of cocaine-induced synaptic rearrangements, I measured the PPR and AMPA/NMDA ratios of the PL afferent-evoked EPSCs (Figure 10A-B). There was no synaptic difference for either PL afferent type between naïve and saline-treated mice (Figure 11). However, the PPR of dMSN-EPSCs, but not that of iMSN-EPSCs, was significantly lower in cocaine-treated mice than in saline-treated mice, suggesting an increase in presynaptic release probability at PL afferent synapses to dMSNs in cocaine-treated mice. In contrast to PPR, the AMPA/NMDA ratios in cocaine-treated mice were not different from those in saline-treated mice in any synaptic type (Figure 10C-F). Therefore, presynaptic alterations are likely to drive the cocaine-induced shift in PL inputs toward dMSNs.

Riluzole precludes an increase in the excitability induced by co-activation of group 1 mGluR and D2R

While D2R activation reduced the excitability of PL L5 PNs (Figure 1), D2-PNs-to-dMSN synapses were strengthened upon repeated cocaine administration (Figure 9 and 10). This synaptic strengthening is unexpected in light of the notion that cocaine elevates the prelimbic DA level by which the excitability of D2-PNs is expected to decrease. However, Gee et al. (2012) showed that D2R activation promotes burst firing of prefrontal thick-tufted L5 PNs (probably ET cells) when the PNs are pre-conditioned with glutamatergic afferent stimulation, but not when under baseline conditions (Gee, Ellwood et al. 2012). This implies that D2R activation may exert differential effects on L5 PNs depending on extracellular glutamate levels. Repeated cocaine treatment increases the extracellular glutamate level in mPFC (Williams and Steketee 2004), and group 1 metabotropic glutamate receptor (mGluR) is necessary for cocaine sensitization (Chiamulera, Epping-Jordan et al. 2001). Therefore, I questioned whether mGluR modulates the effects of D2R on the excitability of D2-PNs. It has been shown that mGluR activation increased the number of spikes induced by depolarizing currents and triggers post-burst persistent activity (PA) in prefrontal ET cells, but not in IT cells

(Kalmbach, Chitwood et al. 2013). I also confirmed these findings in the NAcC-projecting PNs belonging to the IT cell group. Bath-applied 20 μM DHPG, a group1 mGluR agonist, had little effect on the number of spikes induced by 100 pA current injection (Figure 12A). When a post-burst PA was defined as generation of at least 5 AP within 5 s after a 100 pA-induced burst, DHPG did not trigger the post-burst PA in most trials (Figure 12C, 12F). Next, I examined the co-activation effects of mGluR and D2R on the excitability of D2-PNs. Surprisingly, quinpirole, which reduced excitability in the baseline condition (Figure 1), increased the number of spikes under the influence of DHPG (Figure 12B). Thus, co-activation of mGluR and D2R also increased the propensity for post-burst PA generation and duration (Figure 12D, 12G). These results imply that DA may increase the excitability of D2-PNs in cocaine-treated mice, as long as prefrontal glutamate levels are elevated in those mice. Supporting this view, repeated cocaine injection increased the proportion of c-fos(+) cells among NAcC-projecting D2-PNs (Figure 12I-M) as well as among NAcC-projecting D1-PNs (Figure 13).

The data shown in Figure 9 raise a possibility that DA-induced excitability enhancement in D2-PNs may underlie the changes of PL-to-NAcC synaptic strength. Before testing this possibility, I

examined whether riluzole blocks the excitability increase induced by mGluR/D2R co-activation. Riluzole is a clinical drug for amyotrophic lateral sclerosis (Bensimon, Lacomblez et al. 1994), and is also experimentally used to block persistent sodium current ($I_{Na,P}$) known to be critical for neuronal excitability including PA (Le Bon-Jego and Yuste 2007, Katz, Stoler et al. 2018). After confirming that riluzole reduced $I_{Na,P}$ and excitability of NAcC-projecting PNs (Figure 14), I examined the effect of 5 μM riluzole on DHPG/quinpirole treatment-induced excitability changes in D2-PNs. I found that riluzole not only reduced the number of spikes (Figure 12B), but also reversed post-burst PA generation (Figure 12E, 12H).

Reduction of the PL cortical excitability alleviates cocaine-induced alterations in behavior and synaptic strength

I hypothesized that reducing the excitability of PNs in the PL cortex using riluzole would prevent the cocaine-induced LS and rewiring of PL-NAcC connectivity. To test this hypothesis, Hyun Jin Kim (Pohang University of Science and Technology) bilaterally infused either 20 μM riluzole or vehicle in the dorsal part of the PL cortex 10 min before 10 mg/kg cocaine injection for five consecutive days (see Figure 15A for the experimental timeline).

Kim compared the travel distances of subject mice between the vehicle/cocaine and riluzole/cocaine groups, and found that riluzole significantly reduced LS (Figure 15B, C). This riluzole effect was not due to its non-specific sedative effects, because the locomotion activity of subject animals was not significantly affected by the same infusion of riluzole when treated with saline rather than cocaine (Figure 15C). Finally, Kim administered 5 mg/kg riluzole through i.p. injections instead of the local infusion into the PL cortex and confirmed that riluzole i.p. administration also alleviated cocaine-induced LS (Figure 15D, E). Moreover, riluzole i.p. injection prevented conditioned place preference (CPP), which involves synaptic potentiation of ventral hippocampus to D1(+) MSNs of NAcC and arguably mPFC-to-NAcC connection (Otis, Dashew et al. 2013, Zhou, Zhu et al. 2019, Zhou, Yan et al. 2020) (Figure 15F-H), suggesting potential versatile effects of riluzole in alleviating cocaine-induced addiction behaviors.

I also tested whether riluzole infusion into the PL cortex has any effect on cocaine (10 mg/kg)-induced rewiring of PL-NAcC connections associated with its behavioral effects. To this end, I injected AAV-CaMKIIa-ChR2 into the PL cortex, and recorded EPSCs evoked by opto-stimulation of PL afferents in the NAcC fmy weeks later (Figure 16A). The amplitudes of the dMSN-EPSCs

were larger than those of the iMSN-EPSCs in most pairs obtained from subject mice in the vehicle/cocaine group, similar to what is shown in Figure 9. In contrast, no bias of PL inputs to either dMSNs or iMSNs was observed in the riluzole/cocaine group as well as in the riluzole/saline group (Figure 16B – C). Supporting this result, the iMSN/dMSN-EPSC ratios did not differ between the riluzole/cocaine and riluzole/saline groups, whereas those in the vehicle/cocaine group were significantly lower than those in the other two groups (Figure 16G). Importantly, riluzole prevented cocaine-induced reduction in the PPR of dMSN-EPSCs without affecting that of iMSN-EPSCs (Figure 16H), corroborating the involvement of presynaptic mechanisms in cocaine-induced biasing of the PL-to-NAcC connections toward dMSNs. My results substantiate the potential efficacy of riluzole treatment as a candidate therapy for overcoming early behavioral adaptation to addictive drugs.

To ascertain whether the reduced intrinsic excitability of PL PNs is responsible for the riluzole effects on the cocaine-induced rewiring, I reduced the excitability of D1- or D2-PNs using Designer Receptors Exclusively Activated by Designer Drugs (DREADD) techniques (Figure 16D, 17). In agreement with results from riluzole infusion, i.p. injection of CNO (10 mg/kg), a hM4d(G_i)

agonist, prior to the cocaine treatment prevented cocaine-induced alterations of presynaptic strength (Figure 16E-H). These results suggest that the reduction of intrinsic excitability of PL PNs could be a promising strategy for alleviating the development of rewiring associated with drug addiction.

.

Discussion

In the present study, I examined the cocaine-induced changes of PL-NAcC synaptic strength (summarized in Figure 18). I identified prelimbic NAcC-projecting PNs based on their expression of DA receptor types, and NAcC MSNs on their projection targets. I found that both D1R(+) and D2R(+) cells comprise NAcC-projecting PL neurons. These cells displayed similar intrinsic properties, whereas their excitability was regulated in the opposite way by their own DA agonists. D1- and D2-PNs in L5 of the PL cortex unbiasedly innervated dMSNs and iMSNs of the NAcC in the control state, but a biased connection toward dMSNs was set up through presynaptic mechanisms after repeated cocaine administration. This rewiring may be particularly relevant to the early development of LS, as riluzole infusion into the PL cortex alleviated both LS and rewiring. Given that early LS is a manifestation indicating that an animal recognizes the drug as an increasingly salient stimulus, inhibition of early phase LS may be clinically important in that behavioral sensitization may play a role in subsequent drug dependence, such as reinstatement of drug-seeking behaviors (Steketee and Kalivas

2011).

Figure 7 showed little difference between dMSN and iMSN in their intrinsic excitability. Previous studies, however, showed that D1-MSN is more excitable than D2-MSN (Grueter, Brasnjo et al. 2010, Deroche, Lassalle et al. 2020). My results may appear to be not consistent with these studies under the previous notion that D1-MSNs and D2-MSNs in the NAcC largely constitute direct and indirect pathways, respectively, similar to the dorsal striatum. But this notion has been undermined by Kupchik et al. (Kupchik, Brown et al. 2015), which demonstrated that D1-MSNs robustly innervate not only VTA but also VP, while D2-MSNs project to only VP. In light of this study, it is expected that both D1- and D2-MSNs would comprise the iMSN population. Even if D1-MSNs are more excitable than D2-MSNs, D1-MSNs that belong to indirect pathway would dilute the lower excitability of D2-MSNs, resulting in little difference between dMSNs and iMSNs.

Similar to my results, it was previously shown that presynaptic mechanisms underlie cocaine-induced potentiation of mPFC-to-NAc shell synapses (Suska, Lee et al. 2013). A variety of presynaptic LTP (preLTP) mechanisms have been described in various brain regions (Yang and Calakos 2013). While some forms of preLTP can be induced by repetitive presynaptic activity alone,

the majority of preLTP require a co-incident retrograde messenger released from postsynaptic cells, which ensures the input-specific preLTP induction. I showed that infusion of riluzole into the PL cortex prevents cocaine-induced rewiring of PL-NAcC connections, suggesting that remodeling of those syanpses depends on presynaptic neuronal activities. However, synaptic potentiation occurred in dMSNs, but not in iMSNs, regardless of the presynaptic neuron type, implying the requirement of retrograde signaling for the induction of preLTP. The retrograde messenger released from dMSNs, but not iMSNs, remains to be identified. Recently, it was shown that acute cocaine exposure elevated D1-MSN activity but reduced D2-MSN activity (van Zessen, Li et al. 2021). Given that high postsynaptic Ca^{2+} signaling is required for the release of retrograde messengers such as nitric oxide and endocannabinoids (Arancio, Kiebler et al. 1996, Cui, Paille et al. 2015), cocaine-induced activation of dMSN may facilitate the release of a retrograde messenger that mediates preLTP at PL-NAcC synapses. Alternatively, differential expression of LTP between dMSNs and iMSNs may be responsible for the biased rewiring. For example, glutamatergic synaptic activation induces endocannabinoid-mediated LTD in iMSNs, but not in dMSNs (Grueter, Brasnjo et al. 2010). Such a high propensity for LTD induction may inhibit the

strengthening of excitatory synapses in iMSNs.

My results suggest that the D1R- and D2R-expressing cell populations are segregated in NAcC-projecting PL neurons that have similar intrinsic properties. In contrast to my findings, earlier studies reported that mPFC cells expressing D1R have higher R_{in} and smaller hyperpolarization evoked-voltage sag ratios (Gee, Ellwood et al. 2012, Seong and Carter 2012), indicative of smaller hyperpolarization-activated cation currents (I_h) (Dembrow, Chitwood et al. 2010), compared to D2R-expressing cells. The reason for the discrepancy between the present and previous studies might be because I compared D1 and D2-PNs in somewhat homogeneous PN group projecting to the NAcC, unlike previous studies. The majority of L5 NAc-projecting PNs recorded in the present study showed the intrinsic properties similar to IT cells, low voltage sag ratios and high R_{in}, regardless of the expressing DA receptor type (Oswald, Tantirigama et al. 2013).

I found that the excitability of D2-PNs was reduced by D2R activation, whereas that of D1-PNs was increased by D1R activation (Figure 1). Paradoxically, cocaine-induced rewiring toward dMSNs was found both in D1- and D2-PNs (Figure 9). This incongruity could be resolved by my finding that D2-PN excitability is increased by co-activation of D2R and group 1

mGluR (Figure 12). While DHPG increased the spike numbers induced by the depolarizing current and enhanced the post-burst PA in ET cells, it had little effect on the excitability of IT cells (Kalmbach, Chitwood et al. 2013), to which NAcC-projecting PNs belong. The present study showed, however, that co-activation of D2R renders the effects of DHPG on NAcC-projecting cells similar to those on ET cells. Although it is unclear whether co-activation of mGluR and D2R occurs during cocaine administration, previous and present studies support the involvement of mGluR and D2R in cocaine sensitization. First, cocaine administration increased the extracellular DA and glutamate levels in the mPFC (Sorg, Davidson et al. 1997, Williams and Steketee 2004). Second, group 1 mGluRs are essential for cocaine sensitization (Chiamulera, Epping-Jordan et al. 2001). Third, a recent study showed that the inhibition of D2R in the mPFC suppresses cocaine sensitization (Kawahara, Ohnishi et al. 2021). Moreover, because riluzole prevented rewiring not only D1-PNs but also D2-PNs, rewiring of D2-PNs seems to depend on increased presynaptic activity similar to D1-PNs (Figure 16), supporting the view that D2R may play a role in enhancing the excitability of D2-PNs, probably under group 1 mGluR co-activation. The possible molecular mechanism underlying co-activation might be synergistic actions of mGluR1/5 and D2R.

Activation of Gi/o-coupled receptors triggers diverse downstream signaling pathways. $G\alpha_i$ not only inhibits adenylate cyclase but also activates Ras and MAP kinase (Koch, Hawes et al. 1994). Moreover, it is well known that phospholipase $C\beta$ binds not only to $G\alpha_q$ but also the $\beta\gamma$ complex dissociated from trimeric G_i proteins (Murthy, Coy et al. 1996, Rhee 2001, Murthy, Zhou et al. 2004). These interactions target $PLC\beta$ to the vicinity of their substrate to produce IP3 and DAG, which triggers Ca^{2+} release from internal store and activation of PKC. Therefore, G_i- and G_q-coupled receptors synergistically interact in a cell, and coactivation of them often results in supralinear stimulation of $PLC\beta$ (Philip, Kadamur et al. 2010). To my knowledge, synergistic action of G_q and G_i-coupled receptors has been previously observed mostly in non-neuronal cell (Shah, Siddiqui et al. 1999, Philip, Kadamur et al. 2010), although D2-dependent PLC activation has been once shown in striatal MSNs (Hernandez-Lopez, Tkatch et al. 2000). The synergistic action of G_q and G_i-coupled receptors may be a possible explanation why co-activation of mGluR1/5 and D2R enhanced the excitability D2-PNs whereas mGluR1 alone had little effect (Figure 12). In addition to its effects on intrinsic excitability, D2R has been found to facilitate recruitment and summation of polysynaptic excitatory synaptic inputs promoting burst firing in mPFC L5 PNs

(Wang and Goldman-Rakic 2004).

The present study showed that synaptic strength of PL PNs biased to dMSN in the NAcC in the early stage of repeated cocaine administration. It remains, however, to be elucidated whether rewiring of PL-NAcC synapses would persist after a prolonged withdrawal interval and whether similar rewiring occurs after self-administration of cocaine. Suska et al. (2013) comprehensively investigated the quantal changes at IL-to-NAc shell (IL-NAcSh) synapses induced by passive and self- administration (PA and SA) of cocaine with or without a long withdrawal interval (Suska, Lee et al. 2013). This study showed that both PA and SA of cocaine for 5 days increased the release probability (Pr) at IL-NAcSh synapses during not only short-term (1 day) but also prolonged withdrawal intervals (45 days), indicating sustained increase in Pr at least until 45 withdrawal days. Similar to Suska et al (2013), our results suggest that presynaptic mechanisms are responsible for the rewiring at PL-NAcC synapses. These similarity between at PL-NAcC and IL-NAcSh synapses raises a possibility that presynaptic activity-dependent rewiring might occur after SA, and be stable after a prolonged withdrawal, although the possibility should be tested.

In summary, I discovered that two distinct subsets of NAcC-

projecting PL cells (D1− and D2−PNs) unbiasedly innervate dMSNs and iMSNs in naïve brains, but this balanced innervation is disrupted by repeated cocaine exposure, which biases the connection toward the direct pathway through presynaptic mechanisms. Furthermore, I found that this unbalanced connection was closely correlated with LS from the riluzole experiments. Indeed, local infusion of riluzole into the PL cortex prevented cocaine−induced LS and rewiring. Taken together, riluzole can be a candidate therapeutic agent for preventing cocaine sensitization and its underlying synaptic rearrangements.

Materials and methods

Animals and ethical approval

Experiments were carried out using D1-cre hemizygous mice (Tg(Drd1-cre)EY262Gsat/Mmucd; MMRRC #030989-UCD), D2-cre hemizygous mice (Tg(Drd2-cre)ER44Gsat/Mmucd; MMRRC #032108-UCD) crossed with wild-type C57BL/6J mice (purchased from Jackson Laboratory). All animal studies and experimental protocols were approved by the Institutional Animal Care and Use Committee (IACUC, approval No. SNU-190716-6) at Seoul National University. The animals were maintained at standard environmental conditions (25 ± 2 ° C; 12/12 h dark/light cycle) and were housed under veterinary supervision at the Institute for Experimental Animals, Seoul National University College of Medicine.

Surgery

For optical stimulation, I injected 0.7 μl of AAV5-EF1a-double floxed-hChR2(H134R)-EYFP-WPRE-HGHpA (1.03 × 10^{12} vg/ml; addgene #20298) or AAV5-CaMKIIa-hChR2(H134R)-

mCherry (1.03×10^{11} vg/ml; addgene #26975) into mPFC PL of D1-cre, D2-cre mice or wild-type mice. For retrograde labeling, 250 nl (1.0 μg/μl) of Alexa-conjugated Cholera Toxin subunit B (CTB-Alexa 555, CTB-Alexa 647; Invitrogen) was injected into VTA and VP. To perform whole-cell recording selectively at PFC, 0.7 μl of AAV5-Ef1a-DIO EYFP (1.03×10^{12} vg/ml; addgene #27056) was injected into mPFC PL and 250 nl (1.0 μg/μl) of CTB-Alexa 647 was injected to NAcC. Virus and CTB-Alexa were injected into 4-week-old and 6-week-old mice, respectively. Stereotaxic coordinates were (AP, ML, DV; in mm from bregma): +1.65, +0.35, -2.2 for PL; +1.5, +0.85, -4.6 for NAc core; +0.32, +1.3, -5.0 for VP; and -3.3, +0.4, -4.55 for VTA. A syringe pump (WPI, MICRO2T) was used for infusion at 100 nL/min and injection needle was withdrawn 10 min after the end of the infusion. For local riluzole infusion to PL, stainless steel guide cannula (26 gauge; Plastics one) were lowered in the brain of 7-week-old mice (AP: $\pm$1.75, ML: $\pm$0.5, DV: -1.85) and secured to the skull using dental cement (Dentsply sirona). Infusion cannula (33 gauge) extended 0.5 mm past the end of the guide cannula. Riluzole or vehicle (aCSF) were infused at a rate of 250 nL/min for 2min, 10 min before behavioral experiments. Animals were anesthetized with 5% isoflurane for the duration of stereotaxic surgery. Except for the

cannulated groups, subjects were pretreated vehicle (saline) or riluzole (5 mg/kg) 30 minutes before the injection of cocaine or saline treatment.

Cocaine treatment

To obtain electrophysiological data from acute slice of cocaine treated or control mice, cocaine hydrochloride (20 mg/kg; Toronto research chemicals) or saline were injected intraperitoneally (i.p.) to animals once daily for five consecutive days at the same time. On day 6, brain slicing was performed. 10 mg/kg cocaine was used in the behavioral experiment.

Slice preparation

Coronal PFC or NAc slices were obtained from P56–70 mice of both sex. After mice anaesthetized by inhalation with 5% isoflurane, they were decapitated and the brain quickly removed and chilled in an ice-cold high magnesium cutting solution containing the following (in mM): 110 choline chloride, 25 $NaHCO_3$, 20 Glucose, 2.5 KCl, 1.25 NaH_2PO_4, 1 Sodium pyruvate, 0.5 $CaCl_2$, 7 $MgCl_2$, 0.57 Ascorbate, with pH adjusted to 7.4 by saturating with carbogen

(95% O2, 5% CO2), and with osmolality of approximately 300 mOsm/L. The isolated brain was glued onto the stage of a vibrating blade microtome (Leica VT1200) and 300 μm-thick slices were cut. The slices were incubated at 36 ° C for 30 min in the artificial cerebrospinal fluid (aCSF) containing the following (in mM): 125 NaCl, 25 $NaHCO_3$, 20 Glucose, 2.5 KCl, 1.25 NaH_2PO_4, 1 Sodium pyruvate, 2 $CaCl_2$, 1 $MgCl_2$, 0.57 Ascorbate, bubbled with 95% O_2 and 5% CO_2., and thereafter maintained at room temperature.

Whole-cell patch clamp

Whole-cell voltage- or current-clamp recordings were performed at 32 ± 1° C and the rate of aCSF perfusion was maintained at 1-1.5 ml/min. The recordings were made in somata with EPC-10 amplifier (HEKA Electronik) at a sampling rate of 20-25 kHz.

Patch pipettes (3-4 MΩ) for recordings were filled with internal solution containing the following (in mM): 125 Potassium gluconate, 10 KCl, 4 NaCl, 20 HEPES, 1 $MgCl_2$, 4 MgATP, 0.3 NaGTP, 0.1 EGTA (pH 7.3 with KOH). For AMPAR/NMDAR ratio and persistent sodium current experiments, pipettes filled with a Cs-based internal (in mM): 120 Cs-methanesulfonate, 10 CsCl, 10 HEPES, 1 $MgCl_2$, 3 MgATP, 0.4 NaGTP, 5 Na_2 phosphocreatine, 0.1 EGTA, 5

QX-314, 10 tetraethylammonium chloride (TEA) (pH 7.3 with CsOH).

Recordings were made with 50 μM DL-APV (APV) to block NMDARs (not used in AMPA/NMDA current ratio), 100 μM picrotoxin to block $GABA_A$ and 1 μM CGP52432 to block $GABA_B$ bath application. In persistent sodium currents experiments, QX-314 and TEA were not included in internal solution, but 20 mM TEA and 0.2 mM $CdCl_2$ were added to aCSF. I monitored series resistance throughout experiments, and excluded recordings with series resistance >25 MΩ from data analysis. Series resistance was not compensated. All electrophysiology data were recorded exclusively in layer5a of PL in right hemisphere.

To compare synaptic properties between the VTA-projecting cells and VTA-projecting cells of the NAcC, I recorded fluorescent pairs of neurons (CTB-alexa 555, CTB-alexa 647) that were located at the same depth in a slice and within 50 μm of each other. The holding potential was maintained at -70 mV. For optical stimulation, 32 mW/mm^2 470 nm light from a light-emitting diode (LED; Mightex Systems, polygon 400) illuminated the fiber, which was transfected with ChR2 through a 20X 0.5 NA water-immersion objective lens (Olympus, UMPLFLN20XW) for 5 ms. In experiments measuring EPSC amplitudes and PPRs, paired pulses

with 50 ms intervals were delivered every 3s. The first EPSC was defined as the EPSC amplitude, and the PPR was calculated as the ratio of the second EPSC over the first EPSC amplitude. To measure the AMPA/NMDA current ratio, I adjusted the light intensity to evoke 100–300 pA AMPAR EPSCs. The peaks of the +40 mV EPSCs 50 ms after stimulation were determined to be the NMDAR EPSCs. Intrinsic properties were recorded at −65 mV in the mPFC PNs and −75 mV in the NAcC MSNs under the current−clamp mode. The input resistance (R_{in}) and sag ratios were calculated from 500 ms and −50 pA current injections. R_{in} was calculated from the steady−state voltage during the current injection. The voltage sag was defined as the ratio of the maximum to steady−state voltage ($V_{Min}-V_{Baseline}$) / ($V_{Steady}-V_{Baseline}$), where V_{Min} is the minimum peak during the first 25 ms, V_{Steady} is the average of the last 25 ms, and $V_{Baseline}$ is the average of the 25 ms preceding the current injection. A ramp current of 250 pA/s was injected to measure the number of spikes and the thresholds of the MSNs. The AP threshold was defined as the voltage at which dV/dt exceeded 20 V/s. A current of 100 pA for 1 s was injected to measure the number of spikes between the first and second APs in the mPFC PNs. To elicit persistent activity, 20 μM DHPG (or DHPG and quinpirole together) was bath−applied for at least 20 min.

Persistent activity was defined as the maintenance of firing that occurred for 1 min after the 100 pA, 1 s current injection at a membrane potential of −60 mV. If firings did not occur within 5 s after the current injection, or if fewer than five firings occurred, I classified the group as a non−burst group. The point at which the firing stopped for more than 5 s was defined as the termination time. In persistent activity experiments, APV, picrotoxin, and CGP 52432 were not bath−applied. Persistent sodium currents were recorded using a slowly increasing voltage ramp pulse (10 mV/s) from a holding potential of −60 mV to 0 mV in a voltage−clamp configuration. To obtain only tetrodotoxin−sensitive currents, I recorded 1 μM tetrodotoxin bath−applied traces to subtract values from the original trace.

Locomotor activity test

Subjects were acclimated for 2 days by freely moving for 10 min in a test arena (size: 60 cm X 40 cm X 30 cm; white acrylic box), and basal locomotor activity was measured in the second day of acclimation. Subject mice were released in the box center right after either saline or cocaine (10 mg/kg) treatment at the home cage for five sequential days. Movements were recorded with a

video camera for 10 minutes following a 30-second delay for the acclimation every recording day. The recorded movement path in the box was analyzed by the SMART 3.0 video tracking software (PanLab).

Imaging

For fluorescence imaging, mice were anaesthetized and perfused intracardially with phosphate buffered saline (PBS; Gibco, pH 7.4) followed by 4 % paraformaldehyde (PFA; FUJI FILM). Brains were fixed overnight at 4 ° C in 4 % paraformaldehyde. Slices were cut on a vibratome at 100 μm thickness in PBS. Slices were rinsed several times with PBS and were coverslipped using mounting media (Biomeda). All imaging was performed on an Olympus FV1200 confocal microscope.

cFOS immunohistochemistry and cell counting

For selective counting of cFOS in NAcC-projecting D2-PNs, I used Drd2-cre mouse injected AAV-DIO-EYFP and CTB 647 (depicted in "Surgery" section). Saline or cocaine wa injected

intraperitoneally once a day for five consecutive days. After injection, the mice were allowed for freely moving in the open-filed during 10 min. On day 5, 2 hours after intraperitoneally injection, brains were perfused intracardially and post-fixed with 4 % PFA at 4 ° C overnight. The fixed brains were briefly frozen in liquid nitrogen and embedded in optimum cutting temperature compound (OCT; Leica Biosystems) and 30 μm horizontal slices were obtained using a cryostat (Thermo scientific, HM525 NX). After washed in PBS, the slices were blocked with 5 % normal goat serum (NGS) and 0.5 % TritonX-100 in PBS for 1 h at room temperature. 3 % NGS and 0.5% TritonX-100 in PBS was used for primary- and secondary antibody incubation. Rabbit monoclonal anti-cFOS (1:1000; Cell signaling technology, 2250S) was used as primary antibodies. Primary antibody incubation was performed at 4 ° C overnight, followed by 5 min * 6 times PBS wash in room temperature. Goat anti-rabbit Cy3 (1:1000; Invitrogen, #A10520) was used as secondary antibody. Secondary antibody incubation was carried out at room temperature for 3 h, followed by 10 min * 3 times PBS wash. After DAPI staining for 5 mins, slices were washed 5 min * 3 times PBS. Coverslip were applied as a last step using mounting media (Biomeda).

Images used for cell counting were captured through a 20X (NA

0.75) dry objective from a Leica TCS SP8 confocal microscope. I compared number of cFOS expressing cells among co-labeled cells with EYFP and CTB 647. All images processed using the Fiji software (ImageJ, NIH), and cell counting has been performed manually.

Fluorescent In Situ Hybridization

In order to validate cre and D1R/D2R co-expression of NAcC-projecting PNs in the Drd1- and Drd2-Cre mouse, I used 2 recombinase systems. For the cre dependent retrograde expression of flippase, 0.7 μl of retrograde AAV-pEF1a-DIO-FLPo-WPRE-hGHpA (1×10^{12} vg/ml; addgene #87306) was injected into the NAcC. For the flippase dependent labeling, 0.7 μl of AAV5-Ef1a-fDIO mCherry (1×10^{12} vg/ml; addgene #114471) was injected into the PL. After virus injected mice were anesthetized by 5 % isoflurane, they were decapitated and the brains were quickly extracted and was frozen immediately by liquid nitrogen. The frozen tissues were moved directly into a -20 ° C cryostat and were embedded in the OCT. After 1h for equilibrating tissues to -20 ° C, 20 μm coronal slices were obtained using cryostats and mounted onto Superfrost plus slides (Fischer scientific). Until performing in

situ hybridization, obtained slides were stored in −80 ° C deep freezer. After fixation using 4 % PFA, slides were dehydrated by 50 %, 70 %, 100 %, 100% ethanol. Next, Slides were treated with hydrogen peroxide for 10 minutes at room temperature. For primary antibody incubation, the slides were incubated with rabbit polyclonal anti−mCherry (1:100; Abcam, #ab167453) overnight at 4° C using RNA−protein Co−Detection Ancillary kit (Advanced Cell Diagnostics). After primary antibody incubation, I performed remaining step using RNAScope Multiplex Fluorescent Reagent Kit v2 assay, according to standard guideline provided by Advanced Cell Diagnostics. I used Mm−Drd1−C1 (Cat.No 461901) and Mm−Drd2−C2 (Cat.No 406501) probe to detect each mRNA expression. After last blocker step, I used Goat anti−Rabbit IgG−Alexa 488 secondary antibody (1:1000; Invitrogen, #A−11008) for labeling NAcC projecting D1− and D2−PN.

Images used for counting were captured through a 20X water immersion objective (NA 0.95; Olympus, XLUMPlanFI) from an Olympus FV 1200 confocal microscope. I compared number of Drd1−/Drd2 expressing cells among co−labeled cells with Alexa 488. All images processed using the Fiji software (ImageJ, NIH), and cell counting has been performed manually.

Chemogenetics

For DREADD experiments, I injected CTB-647 and CTB-555 into VP and VTA, respectively. 0.7 μl mixture of AAV5-EF1a-double floxed-hChR2(H134R)-EYFP-WPRE-HGHpA (1.03×10^{12} vg/ml) and AAV9-hsyn-fDIO-hM4D(G_i)-mCherry-hGH polyA (1×10^{12} vg/ml; BrainVTA, #PT-0170) was injected into the PL and 0.7 μl of retrograde AAV-pEF1a-DIO-FLPo-WPRE-hGHpA (1×10^{12} vg/ml; addgene #87306) was injected into the NAcC of Drd1- and Drd2-cre mouse. To validate expression of hM4D(G_i), 10 μM Clozapine N-Oxide dihydrochloride (CNO; Hello bio, #HB6149) was bath-applied 5 min after beginning of whole-cell recording. The CNO induced membrane potential change was recorded 3 min after CNO bath application. To record inhibition effect of PL-PN on cocaine-induced rewiring, 10 mg/kg cocaine was injected intraperitoneally 30 min after i.p injection of vehicle or 10 mg/kg CNO for five consecutive days. To compare CNO effect on cocaine-induced rewiring, I performed patch clamp recording, as description in "Whole-cell patch clamp" section.

Cocaine conditioned place preference (CPP) test

The apparatus for the cocaine CPP test consists of three compartments (White and Black-lined wall chamber: 20 cm × 20 cm, corridor: 20 cm × 10 cm), and a paradigm composed of three phases (acclimation, conditioning, and test phase). During two days of acclimation to the test arena, subjects were freely moving for 15 min in three-compartment apparatus after sham intraperitoneal (i.p.) injection at AM and PM (12hr interval). During the last acclimation session, conduct pre-test recording as basal preference. From the pre-test recording, preferred side of the chamber was assigned as saline pairing and the other side with cocaine. CPP score is defined as the different time duration of cocaine paired and saline paired sides. Subjects were renounced if subjects showed extremely biased (over 70% time duration) to one side of the chamber. During three days of the conditioning phase, subjects were treated with vehicle (0.9% saline) or riluzole (5 mg/kg) by i.p. injection at the home cage 30 minutes before each session. During the conditioning, all chambers were closed, and subjects were released at the center of the corresponding chamber right after a single treatment with saline (0.9% saline) or cocaine (10mg/kg) daily at AM and PM. 24 hrs after the last treatment, the test phase was conducted, and subjects were freely moving for 15 min in

three-compartment apparatus without treatment.

Data Analysis

All data were presented as mean ± standard error of the mean (SEM). Statistical analysis was performed using IgorPro (version 7.08, WaveMetrics) and SPSS (version 26, IBM). Unless otherwise stated, nonparametric Mann-Whitney U test was used to compare non-paired groups, and paired sample t test was used to compare paired groups, respectively. Travel distance data was assessed using Greenhouse-Geisser corrected repeated measures ANOVA followed by Bonferroni's post hoc tests. P-values of < 0.05 were considered statistically significant.

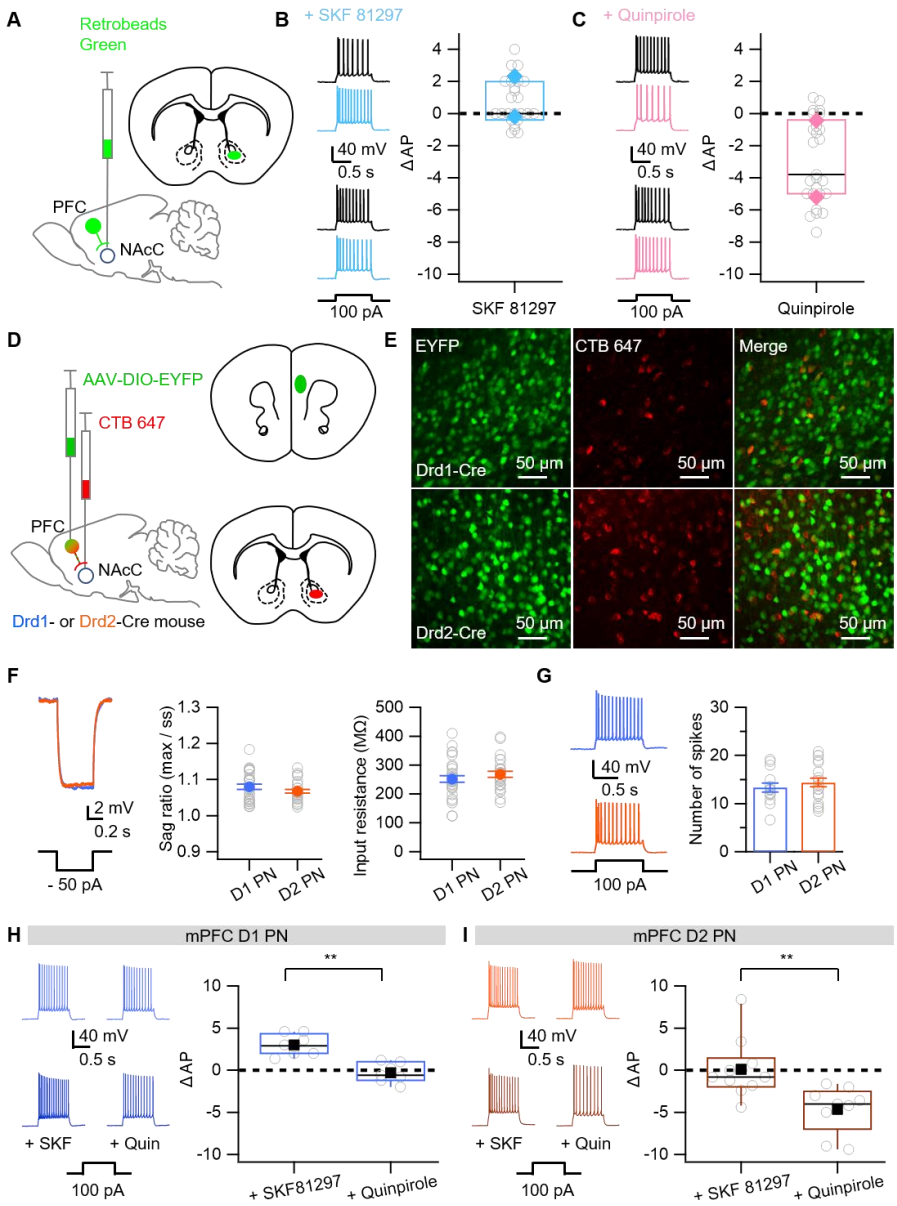
A
Retrobeads
Green
PFC
NAcC
B
+ SKF 81297
40 mV
0.5 s
100 pA
ΔAP
SKF 81297
C
+ Quinpirole
40 mV
0.5 s
100 pA
ΔAP
Quinpirole
D
AAV-DIO-EYFP
CTB 647
PFC
NAcC
Drd1- or Drd2-Cre mouse
E
EYFP
CTB 647
Merge
Drd1-Cre
Drd2-Cre
50 μm
F
2 mV
0.2 s
- 50 pA
Sag ratio (max / ss)
Input resistance (MΩ)
D1 PN
D2 PN
G
40 mV
0.5 s
100 pA
Number of spikes
D1 PN
D2 PN
H
mPFC D1 PN
40 mV
0.5 s
+ SKF
+ Quin
100 pA
ΔAP
**
+ SKF81297
+ Quinpirole
I
mPFC D2 PN
40 mV
0.5 s
+ SKF
+ Quin
100 pA
ΔAP
**
+ SKF 81297
+ Quinpirole

Figure 1. Two populations of prelimbic neurons projecting to NAcC.

(A) Schematic of Retrobead Green injection into the NAc core (NAcC). (B–C) Effects of SKF 81297 (10 μM, D1 agonist, B) and quinpirole (10 μM, D2 agonist, C) on spike numbers elicited by 100 pA depolarizing current in NAcC-projecting PL L5 pyramidal neurons (PNs). *Left insets*, representative traces before (black) and after (colored) bath-application of each agonist. Note that the changes in number of APs (⊿AP) were bimodal. The representative traces for responding and non-responding cells are shown as upper and lower pairs in the left inset. The median values for ⊿AP for SKF 81297 and quinpirole were 0 (n = 25) and −3.8 (n = 27), respectively. The centroids of the bimodal distribution obtained from K-mean clustering are marked with diamond symbols (D1 agonist : 2.32, −0.2; D2 agonist : −5.21, −0.43). (D) Schematic for injections of CTB-647 (red) into the NAcC for retrograde tracing and AAV-DIO-EYFP (green) into the PL for labeling of D1 receptor (D1R) or D2 receptor (D2R)-expressing pyramidal neurons (D1 or D2-PNs) in Drd1-cre or Drd2-cre mice, respectively. (E) Confocal images of labeled L5 PL neurons in a Drd1-cre mouse (upper row) and a Drd2-cre mouse (lower row) that are projecting to NAcC. (F) Subthreshold electrical properties of D1- and D2-PNs. *Left*, representative traces of a D1-PN (blue)

and a D2−PN (orange) in response to −50 pA hyperpolarizing current. *Middle*, mean sag ratios (D1−PNs, 1.08 ± 0.007, n = 31; D2−PNs, 1.07 ± 0.005, n = 27, p = 0.346), *Right*, mean input resistance (D1−PNs, 252.11 ± 11.63 MΩ, n = 31; D2−PNs, 267.77 ± 10.42 MΩ, n = 27, p = 0.27). **(G)** Suprathreshold electrical properties of D1−PNs and D2−PNs. *Left*; representative voltage responses to 100 pA depolarizing current. *Right*, mean number of spikes (D1−PNs, 13.34 ± 0.93, n = 14; D2−PNs, 14.37 ± 0.9, n = 19, p = 0.42). **(H−I)** Effect of SKF 81297 and quinpirole on the number of spikes evoked by the 100 pA depolarizing current in D1− (H) and D2−PNs (I). *Left*, representative traces before (upper) and after (lower) bath application of each agonist. *Right*, summary for ⊿AP in D1−PNs (H; SKF 81297, 3 ± 0.37, n = 8; Quinpirole, −0.31 ± 0.44, n = 7, p <0.01), and D2−PNs (I, Quinpirole, − 4.64 ± 0.93, n = 9; SKF 81297, 0.12 ± 1.12, n = 10, p <0.01). The box plots depict the median and quartiles. The mean value is indicated by a filled rectangle in each box plot. The others are presented as mean ± SEM, $^{*}p < 0.05$, $^{**}p < 0.01$

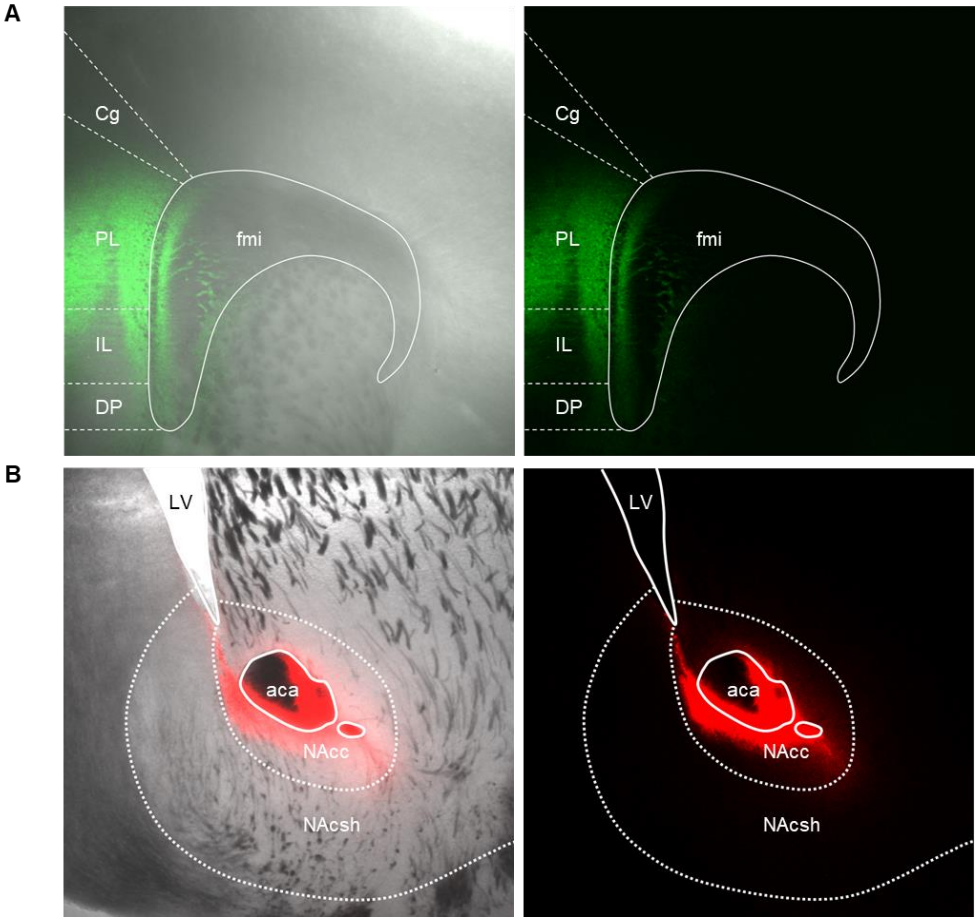
A
Cg
PL
fmi
IL
DP
Cg
PL
fmi
IL
DP
B
LV
aca
NAcc
NAcsh
LV
aca
NAcc
NAcsh

Figure 2. Histology of injection sites in mPFC PL and in NAcC related to Figure 1.

(A) AAV5-Ef1a-DIO EYFP was injected to mPFC PL (green). **(B)** CTB-Alexa 647 was injected to NAc core (red). Abbreviation: Cg, Cingulate cortex; PL, Prelimbic cortex; IL, Infralimbic cortex; DP, Dorsal Peduncular cortex; fmi, forceps minor of the corpus callosum; Cpu, Caudate putamen; aca, anterior commissure anterior part; LV, Lateral Ventricle; NAcC, Nucleus Accumbens Core; NAcSh, Nucleus Accumbens Shell

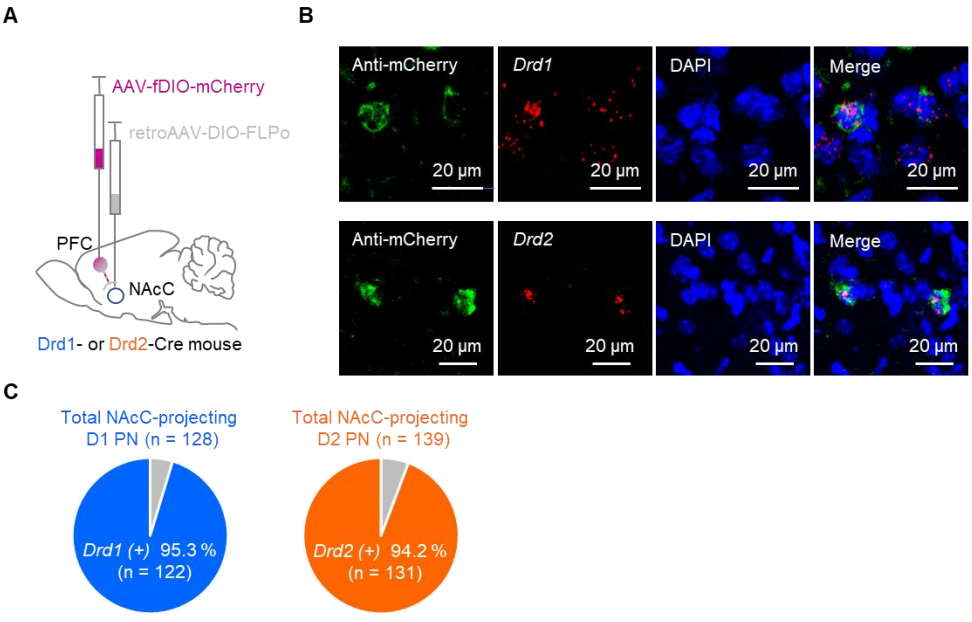
A
AAV-fDIO-mCherry
retroAAV-DIO-FLPo
PFC
NAcC
Drd1- or Drd2-Cre mouse
B
Anti-mCherry
Drd1
DAPI
Merge
20 μm
Anti-mCherry
Drd2
DAPI
Merge
20 μm
C
Total NAcC-projecting
D1 PN (n = 128)
Drd1 (+) 95.3 %
(n = 122)
Total NAcC-projecting
D2 PN (n = 139)
Drd2 (+) 94.2 %
(n = 131)

Figure 3. Validation of cre and D1R/D2R co-expression of NAcC-projecting PNs in the Drd1- and Drd2-Cre mouse.

(A) Schematic for the cre recombinase dependent labeling of NAcC-projecting PNs in the PL expressing D1R or D2R. For the cre dependent retrograde expression of flippase, retrograde AAV-DIO-FLPo was injected into the NAcC. For the filppase dependent labeling, AAV-fDIO-mCherry was injected into the PL. **(B)** *Upper*, Cre dependently mCherry-labeled NAcC-projecting PNs express Drd1 mRNA in Drd1-cre mice. *Lower*, the same as upper but Drd2 mRNA in Drd2-cre mice. **(C)** Proportions for overlapped expression of Drd1 (Left) or Drd2(Right) transcripts among cre or mCherry(+) cells in Drd1- and Drd2-Cre mice, respectively.

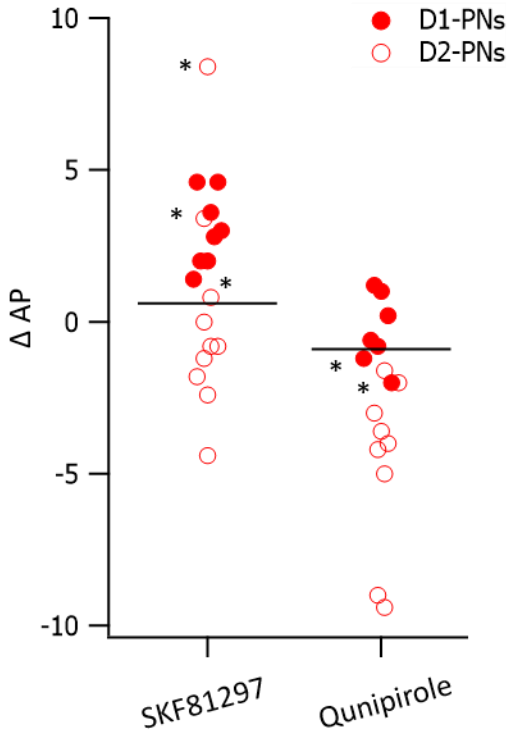
D1-PNs
D2-PNs
10
5
0
-5
-10
Δ AP
SKF81297
Qunipirole

Figure 4. SKF81297 or quinpirole-induced changes in the number of APs elicited 100 pA current injection (ΔAP) in D1- and D2-PNs.

⊿AP from the two PN groups were plotted with respect to each DA agonist to evaluate co-expression of D1- and D2R in a single NAcC-projecting PN. The ΔAP data are reproduced from Figure 1H-I. The horizontal bars indicate the lower margin of 2 S.D. range of ΔAP values induced by SKF81297 in D1-PNs (left) and the upper margin of ΔAP values induced by quinpirole in D2-PNs (right). Because of high variance of the quinpirole effects on ΔAP in D2-PNs, mean and S.D. were calculated without the two outlier points. In five (denoted by asterisk) out of 34 PNs, ΔAP were in the ΔAP range of the other PN group.

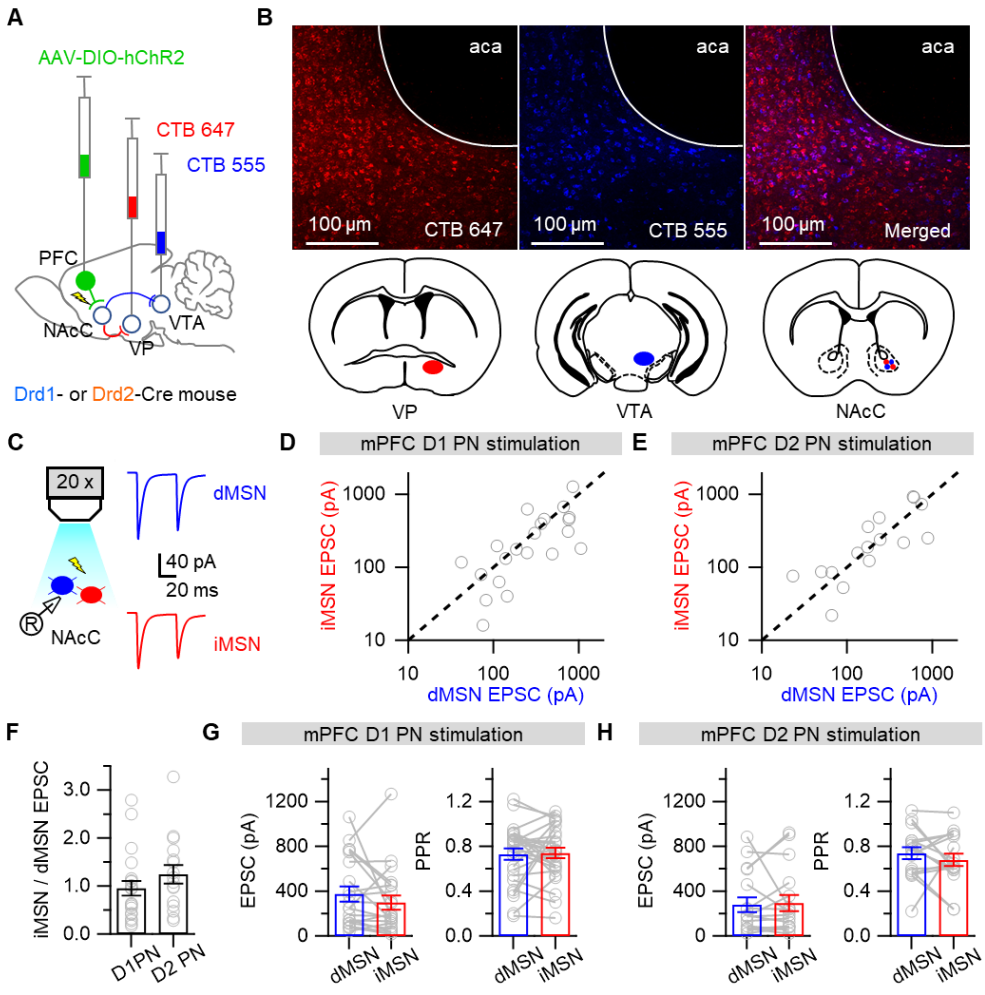
A
AAV-DIO-hChR2
CTB 647
CTB 555
PFC
NAcC
VTA
VP
Drd1- or Drd2-Cre mouse
B
aca
aca
aca
100 μm
CTB 647
100 μm
CTB 555
100 μm
Merged
VP
VTA
NAcC
C
20 x
dMSN
40 pA
20 ms
NAcC
iMSN
D
mPFC D1 PN stimulation
iMSN EPSC (pA)
dMSN EPSC (pA)
E
mPFC D2 PN stimulation
iMSN EPSC (pA)
dMSN EPSC (pA)
F
iMSN / dMSN EPSC
D1PN
D2 PN
G
mPFC D1 PN stimulation
EPSC (pA)
PPR
dMSN
iMSN
H
mPFC D2 PN stimulation
EPSC (pA)
PPR
dMSN
iMSN

Figure 5. Selective opto-stimulation of D1- or D2-PN axon fibers projecting to dMSNs or iMSNs in NAcC.

(A) Schematic for the retrograde labeling of the MSNs and the expression of ChR2 in PL neurons. For retrograde labeling of iMSNs and dMSNs, CTB-647 (red) and CTB-555 (blue) were injected into VP and VTA, respectively. For selective opto-stimulation of D1 or D2-PNs, AAV-DIO-hChR2 was injected into the PL cortex of D1-cre mice or D2-cre mice. **(B)** *Upper*, confocal images of iMSNs (red) and dMSNs (blue) in the coronal slice of NAc. *Lower*, injection sites in the VP (left) and VTA (right), and the locations of the labeled cells in NAcC (right). **(C)** Experimental configuration for comparing light evoked EPSCs measured in neighboring dMSN and iMSN pairs on the same slice. **(D-E)** Plots of iMSN *vs*. dMSN EPSC amplitudes (log scale) evoked by optical stimulation of axon fibers of D1 (D) or D2 (E) cells. **(F)** Ratio of iMSN/dMSN EPSC amplitudes (D1-PNs, 0.95 ± 0.15, n = 21; D2-PNs, 1.24 ± 0.19, n = 16, p = 0.133). **(G-H)** Summary of the evoked EPSC amplitudes (left) and PPRs (right) measured in dMSN and iMSN pairs. EPSCs were evoked by optical stimulation of axon fibers from D1-PNs (G; amplitude, dMSN = 374.87 ± 68.04 pA; iMSN =299.34 ± 64.23 pA, n = 21, p = 0.22; PPR, dMSN = 0.73 ± 0.05; iMSN = 0.74 ± 0.05, n=21, p = 0.82) or D2-PNs (H;

amplitude, dMSN= 279.18 ± 66.61 pA; iMSN= 293.49 ± 70.9 pA, n = 16, p = 0.79; PPR, dMSN = 0.74 ± 0.05; iMSN = 0.68 ± 0.06, n=16, p = 0.35). Data are shown as mean ± SEM.

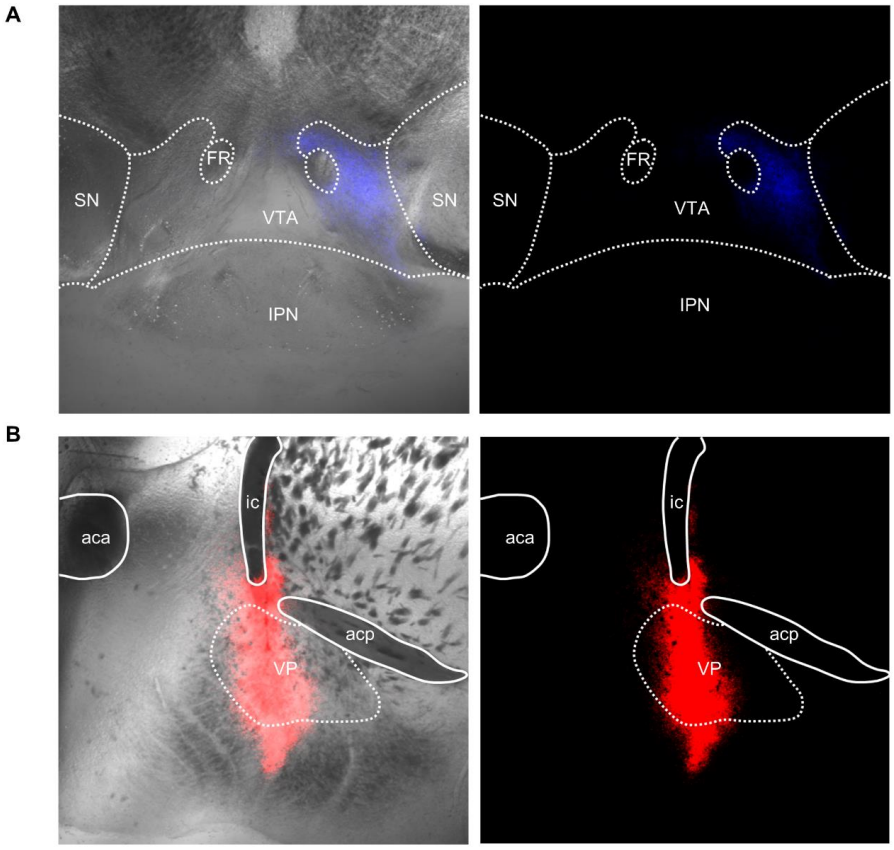
A
FR
SN
VTA
SN
IPN
FR
SN
VTA
IPN
B
ic
aca
acp
VP
ic
aca
acp
VP

Figure 6. Histology for injection sites in VTA and VP related to Figure 2.

(A) CTB-Alexa 555 was injected to VTA (blue). **(B)** CTB-Alexa 647 was injected to VP (red). Abbreviations: aca, anterior commissure anterior part; acp, anterior commissure posterior part; FR, Fasciculus Retroflexus; ic, internal capsule; IPN, Interpeduncular Nucleus; SN, Substantia Nigra; VP, Ventral Pallidum; VTA, Ventral Tegmental Area.

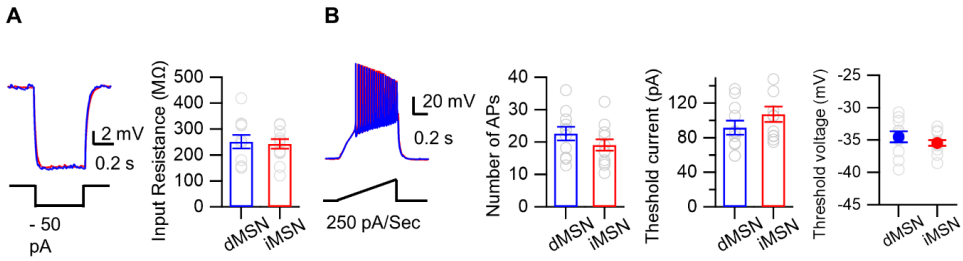
A
2 mV
0.2 s
- 50
pA
Input Resistance (MΩ)
500
400
300
200
100
0
dMSN
iMSN
B
20 mV
0.2 s
250 pA/Sec
Number of APs
40
30
20
10
0
dMSN
iMSN
Theshold current (pA)
120
80
40
0
dMSN
iMSN
Threshold voltage (mV)
-25
-30
-35
-40
-45
dMSN
iMSN

Figure 7. Intrinsic properties of dMSNs and iMSNs measured from voltage responses to −50 pA hyperpolarizing current or ramp current (B) injection.

(A) *Left*, representative traces. *Right*, summary for input resistance of dMSNs and iMSNs (dMSN, 251.28 ± 26.19 MΩ, n = 11; iMSN, 242.96 ± 18.59 MΩ, n = 12; p = 0.9). (B) *Left*, representative traces. Right three plots show the summary for number of spikes (dMSN = 22.6 ± 2.11, n = 11; iMSN = 19.12 ± 1.79, n = 12, p = 0.19), threshold current (dMSN = 91.61 ± 8.13 pA, n = 11; iMSN = 107.09 ± 8.76 pA, n = 12, p = 0.22) and threshold voltage (dMSN = −34.52 ± 0.83 mV, n = 11; iMSN = −35.47 ± 0.46 MΩ, n = 12, p = 0.2) measured from the ramp pulse responses. Current and voltage threshold were defined as the current and voltage at which d*V*/d*t* exceeded 20 V/s. Data are shown as mean ± SEM.

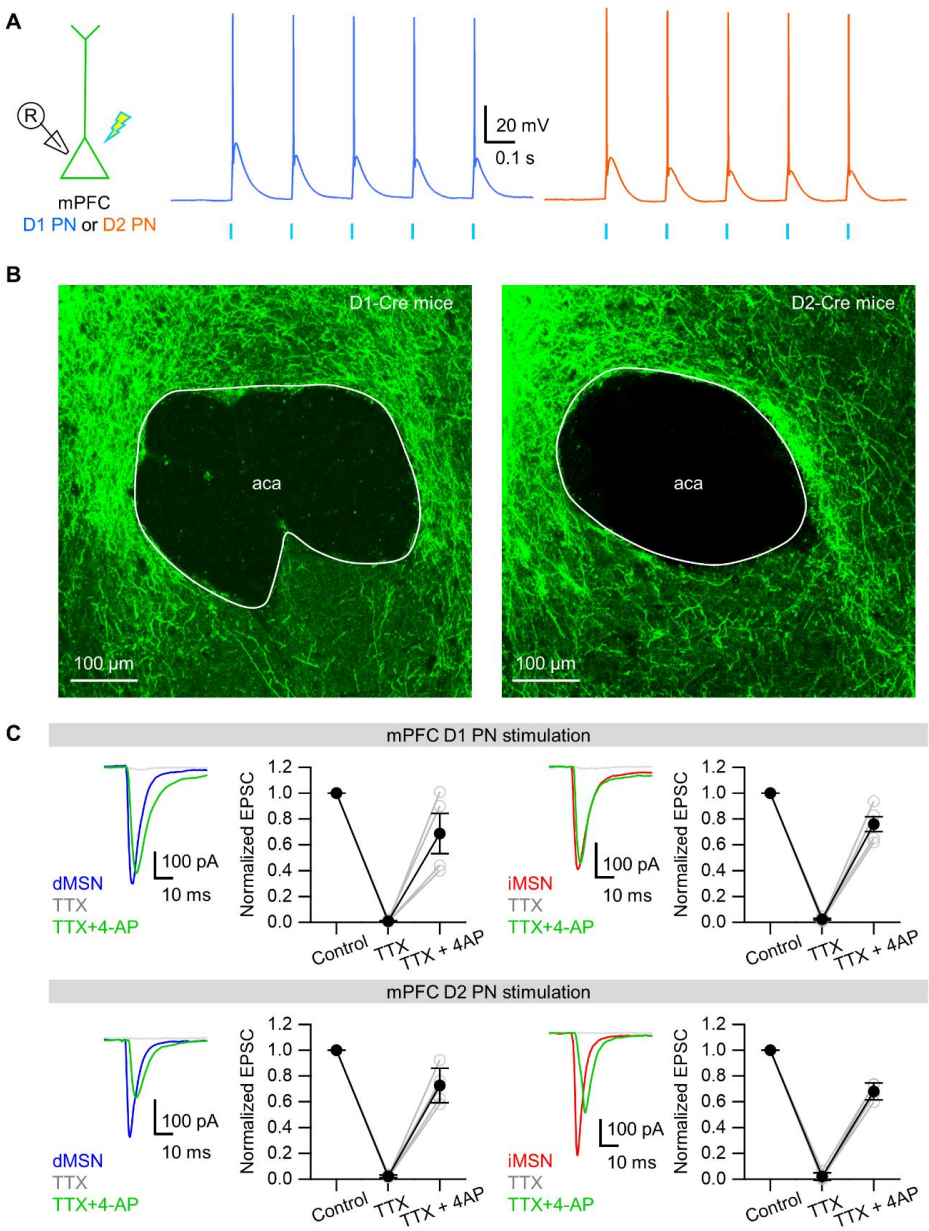
A
R
mPFC
D1 PN or D2 PN
20 mV
0.1 s
B
D1-Cre mice
aca
100 μm
D2-Cre mice
aca
100 μm
C
mPFC D1 PN stimulation
dMSN
TTX
TTX+4-AP
100 pA
10 ms
Normalized EPSC
Control
TTX
TTX + 4AP
iMSN
TTX
TTX+4-AP
100 pA
10 ms
Normalized EPSC
Control
TTX
TTX + 4AP
mPFC D2 PN stimulation
dMSN
TTX
TTX+4-AP
100 pA
10 ms
Normalized EPSC
Control
TTX
TTX + 4AP
iMSN
TTX
TTX+4-AP
100 pA
10 ms
Normalized EPSC
Control
TTX
TTX + 4AP

Figure 8. The light-evoked synaptic events were monosynaptic.

(A) *Left*, experimental configuration showing current clamp recordings of D1 or D2-PNs in L5 of the PL cortex with light stimulation. The middle and right panels show the representative voltage responses in D1-PNs (middle, blue) and D2-PNs (right, orange) evoked by light pulse stimulations (bottom ticks). (B) Axon fibers of D1 (left) and D2-PNs (right) around the NAc. (C) Control-normalized EPSC amplitudes in MSNs. EPSCs were evoked by optostimulation of axon fibers from D1 (upper) or D2 (lower) cells under control conditions or in the presence of TTX or TTX plus 4-aminopyridine (4AP) [For D1→ dMSN, TTX = 0.9 %, TTX+4AP = 68.7 %, n=4; For D1→ iMSN, TTX = 2.3 %, TTX+4AP = 76 %, n=4; For D2→dMSN, TTX = 2.3 %, TTX+4AP = 72.5 %, n=5, For D2→iMSN, TTX = 2 %, TTX+4AP = 68 %, n=4). Data are shown as mean ± SEM.

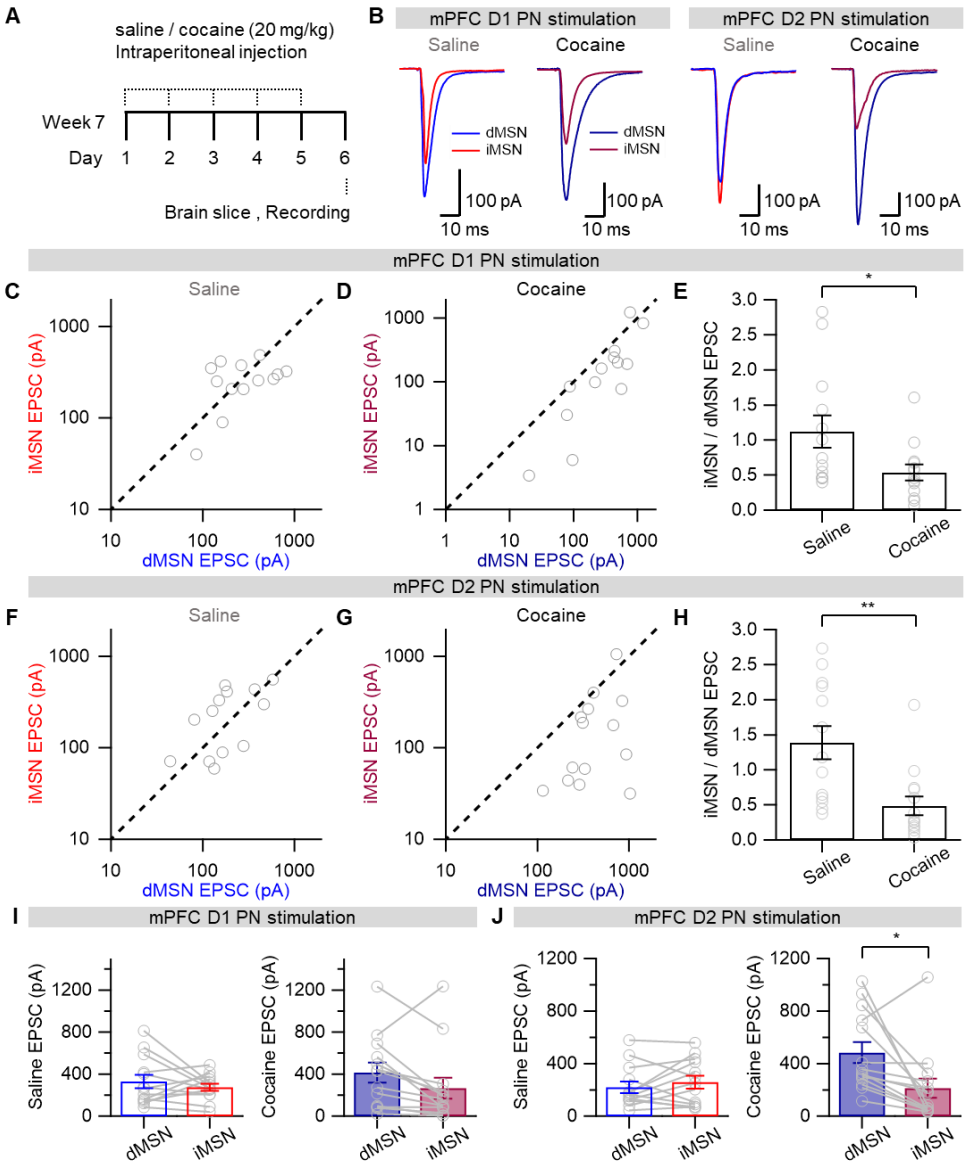
A
saline / cocaine (20 mg/kg)
Intraperitoneal injection
Week 7
Day 1 2 3 4 5 6
Brain slice , Recording
B
mPFC D1 PN stimulation
mPFC D2 PN stimulation
Saline
Cocaine
dMSN
iMSN
100 pA
10 ms
mPFC D1 PN stimulation
C
Saline
D
Cocaine
iMSN EPSC (pA)
dMSN EPSC (pA)
E
iMSN / dMSN EPSC
Saline
Cocaine
mPFC D2 PN stimulation
F
G
H
I
mPFC D1 PN stimulation
J
mPFC D2 PN stimulation
Saline EPSC (pA)
Cocaine EPSC (pA)
dMSN
iMSN

Figure 9. Cocaine-induced rewiring of connections from the PL cortex to the NAcC.

(A) Schematic of the cocaine sensitization protocol. Cocaine or saline was injected intraperitoneally once a day for five consecutive days. On day 6, brain slices were obtained for electrophysiological recording. **(B)** Representative traces of EPSCs evoked by optostimulation of D1 or D2-PN axons, as recorded in neighboring dMSN (blue) and iMSN (red) pairs in the same slices from saline-treated (bright color) or cocaine- treated (dark color) mice. **(C-D)** A plot of iMSN- *vs.* dMSN-EPSC amplitudes (log scale) evoked by opto-stimulation of D1-PN axons in the saline- (C) and cocaine-treated (D) mice. **(E)** Corresponding iMSN/dMSN EPSC amplitude ratio measured in saline- and cocaine-treated mice (saline, 1.12 ± 0.23, n = 13; cocaine, 0.53 ± 0.11, n = 13, $p < 0.05$). **(F-G)** A plot of iMSN- vs dMSN-EPSC amplitudes (log scale) evoked by optical stimulation of D2-PN axons in saline- (F) or cocaine-treated (G) mice. **(H)** Corresponding iMSN/dMSN EPSC amplitude ratio (saline, 1.42 ± 0.24, n = 13; cocaine, 0.45 ± 0.11, n = 14, $p < 0.01$). **(I)** Summary of the amplitudes of the D1-PN stimulation-evoked EPSCs in the dMSN and iMSN pairs of saline-treated (*left*; dMSN, 330.38 ± 63.82 pA; iMSN, 274.51 ± 34.27 pA, n = 13, p = 0.39) and cocaine-treated mice (*right*; dMSN, 414.9 ± 96.03

pA; iMSN, 267.23 ± 100.42 pA, n = 13, p =0.055) **(J)** Summary of the D2−PN stimulation−evoked EPSC amplitudes in the dMSNs and iMSNs in the saline−treated (*left*, 220.6 ± 43.94 pA; iMSN, 272.05 ± 53.94 pA, n = 13, p = 0.26) and cocaine−treated mice (right, dMSN, 484.02 ± 79.16 pA; iMSN, 212.93 ± 72.32 pA, n = 13, $p < 0.05$). Data are shown as mean ± SEM. $^{*}p < 0.05$, $^{**}p < 0.01$.

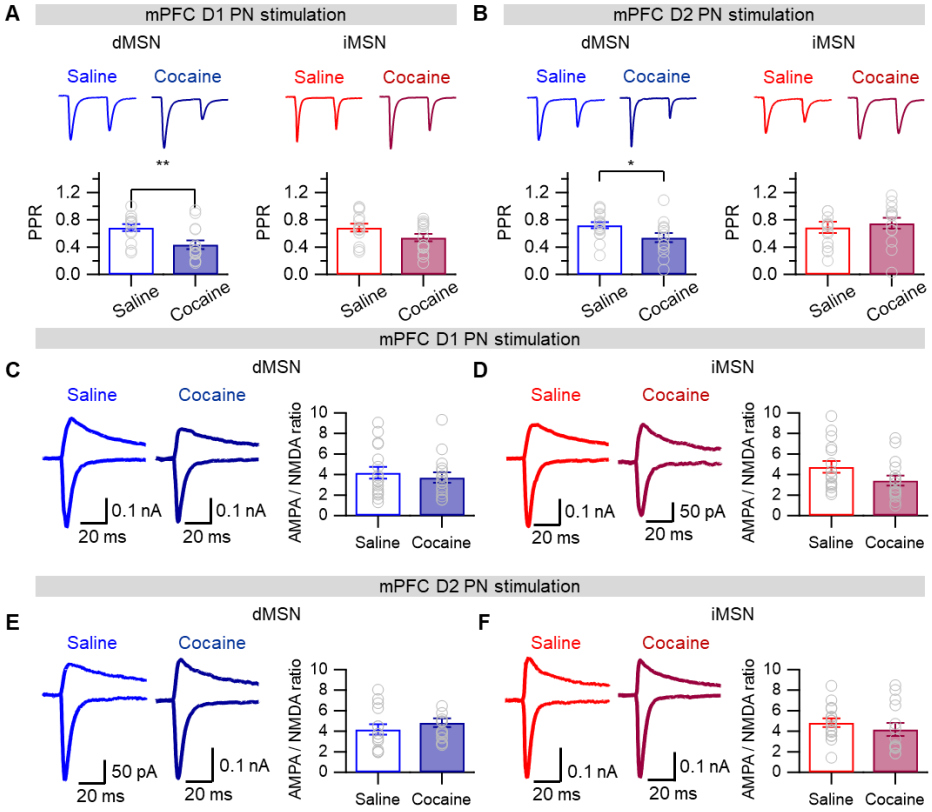
A
mPFC D1 PN stimulation
dMSN
iMSN
Saline
Cocaine
PPR
B
mPFC D2 PN stimulation
C
D
E
F
AMPA / NMDA ratio
0.1 nA
50 pA
20 ms

Figure 10. Presynaptic locus of cocaine-induced plastic changes at PL-NAcC synapses.

(A) PPRs of D1-PN stimulation-evoked EPSCs in saline- and cocaine-treated mice. *Left*, PPRs of dMSN-EPSCs (saline, 0.69 ± 0.05, n = 14; cocaine, 0.43 ± 0.06, n = 15, $p < 0.01$). *Right*, PPRs of iMSN-EPSCs (saline, 0.69 ± 0.06, n = 14; cocaine, 0.54 ± 0.06, n = 15, p = 0.16). **(B)** Same as in *A* but with D2-PN stimulation. *Left*, PPRs of dMSNs (saline, 0.72 ± 0.05, n = 17; cocaine, 0.54 ± 0.07, n = 14, $p < 0.05$). *Right*, PPRs of iMSNs (saline, 0.69 ± 0.08, n = 17; cocaine, 0.75 ± 0.08, n = 14, p = 0.24). *Upper insets*, representative EPSC traces evoked by paired pulses. **(C-D)** Representative traces for EPSCs at −70 and +40 mV, which were evoked by optostimulation of D1-PN axons measured in dMSNs (C) and iMSNs (D) of saline- (left traces) and cocaine-treated (right traces) mice. Bar graphs, AMPA/NMDA ratios of dMSN-EPSCs (C) (saline, 4.16 ± 0.58, n = 17; cocaine, 4.73 ± 0.58, n = 16, p = 0.68) and in iMSN-EPSCs (D) (saline, 3.72 ± 0.5, n = 16; cocaine, 3.42 ± 0.48, n = 16, p = 0.076). **(E-F)** EPSC traces are same as in *C* and *D* but with D2-PN stimulation. Bar graphs, AMPA/NMDA ratios in dMSNs (E) (saline, 4.17 ± 0.52, n = 15; cocaine, 4.82 ± 0.42, n = 16, p = 0.27) and in iMSNs (F) (saline, 4.82 ± 0.42, n = 15; cocaine, 4.18 ± 0.64, n =

14, p = 0.24). Data are shown as mean ± SEM. *p < 0.05, **p < 0.01

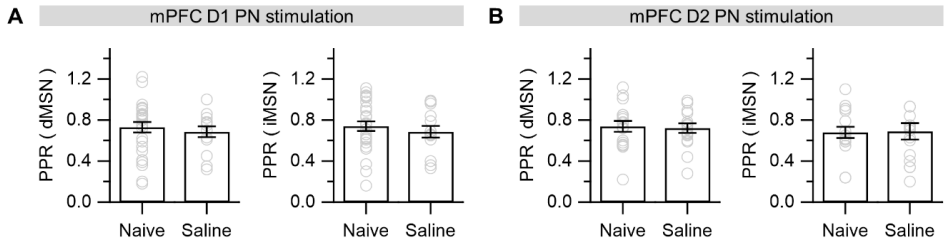
A
mPFC D1 PN stimulation
PPR (dMSN)
1.2
0.8
0.4
0.0
Naive
Saline
PPR (iMSN)
1.2
0.8
0.4
0.0
Naive
Saline
B
mPFC D2 PN stimulation
PPR (dMSN)
1.2
0.8
0.4
0.0
Naive
Saline
PPR (iMSN)
1.2
0.8
0.4
0.0
Naive
Saline

Figure 11. No change of PPR in dMSN and iMSN by repeated saline injection.

(A) Summary for PPR of EPSCs evoked by D1−PN stimulation measured in dMSN (*left*; naïve = 0.73 ± 0.05, n = 27; saline = 0.69 ± 0.05, n = 14; p = 0.3) and in iMSN (*right*; naïve = 0.74 ± 0.05, n = 27; saline = 0.69 ± 0.06, n = 14; p = 0.45). **(B)** same as A but D2−PN stimulation. *Left*, PPR in dMSN (naïve = 0.74 ± 0.05, n = 17; saline = 0.72 ± 0.05, n = 17; p = 0.82). *Right*, PPR in iMSN (naïve = 0.68 ± 0.06, n = 17; saline = 0.69 ± 0.08, n = 17; p = 0.95). Data are shown as mean ± SEM.

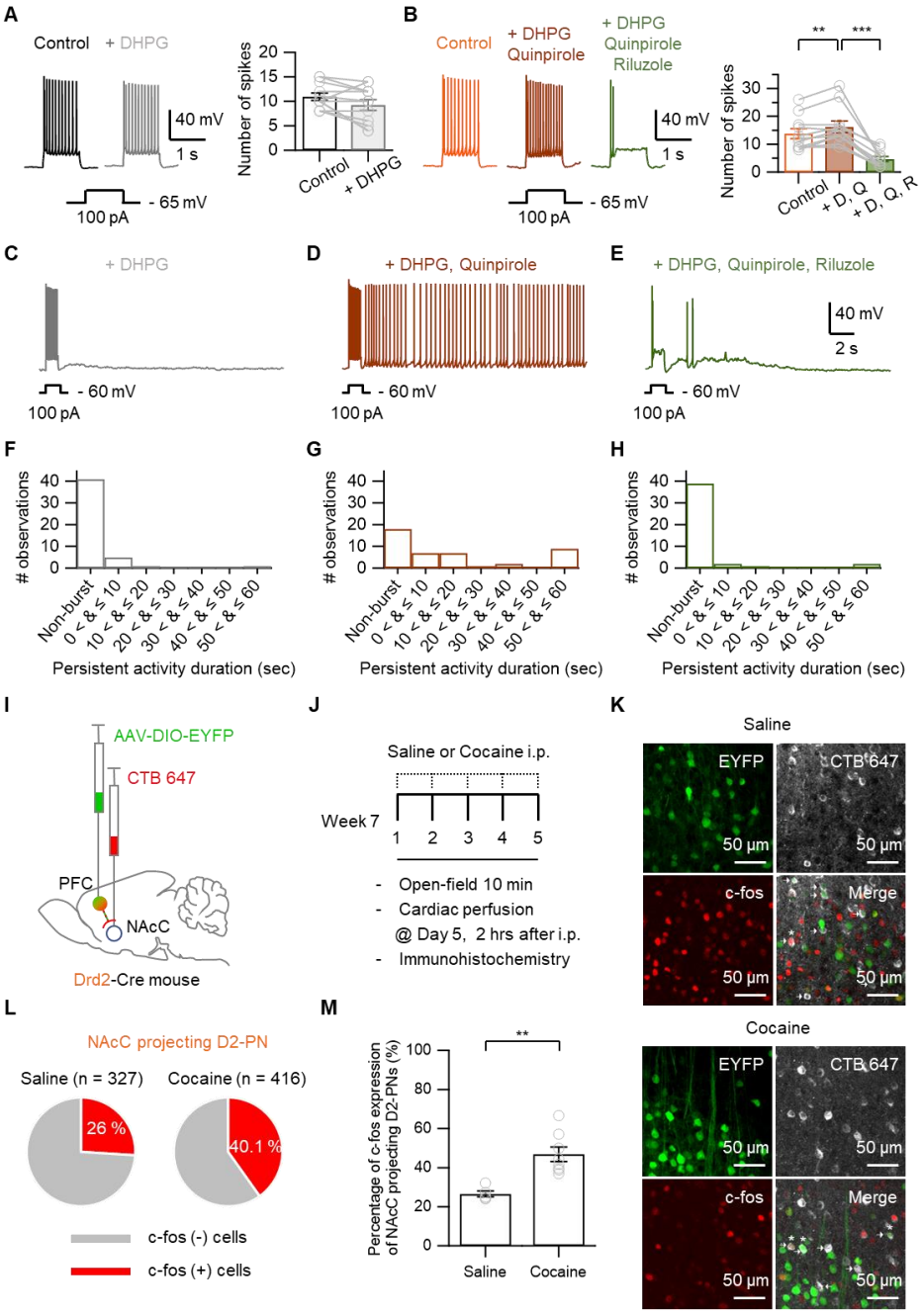
A
Control
+ DHPG
40 mV
1 s
- 65 mV
100 pA
Number of spikes
Control
+ DHPG
B
Control
+ DHPG
Quinpirole
+ DHPG
Quinpirole
Riluzole
40 mV
1 s
- 65 mV
100 pA
**
***
Number of spikes
Control
+ D, Q
+ D, Q, R
C
+ DHPG
- 60 mV
100 pA
D
+ DHPG, Quinpirole
- 60 mV
100 pA
E
+ DHPG, Quinpirole, Riluzole
40 mV
2 s
- 60 mV
100 pA
F
observations
Non-burst
0 < & ≤ 10
10 < & ≤ 20
20 < & ≤ 30
30 < & ≤ 40
40 < & ≤ 50
50 < & ≤ 60
Persistent activity duration (sec)
G
observations
Persistent activity duration (sec)
H
observations
Persistent activity duration (sec)
I
AAV-DIO-EYFP
CTB 647
PFC
NAcC
Drd2-Cre mouse
J
Saline or Cocaine i.p.
Week 7
1 2 3 4 5
- Open-field 10 min
- Cardiac perfusion
@ Day 5, 2 hrs after i.p.
- Immunohistochemistry
K
Saline
EYFP
CTB 647
c-fos
Merge
50 μm
Cocaine
L
NAcC projecting D2-PN
Saline (n = 327)
Cocaine (n = 416)
26 %
40.1 %
c-fos (-) cells
c-fos (+) cells
M
**
Percentage of c-fos expression of NAcC projecting D2-PNs (%)
Saline
Cocaine

Figure 12. Co-activation of D2R and group1 mGluR increases the excitability of D2-PNs.

(A) Effects of DHPG on the number of spikes evoked by the 100 pA depolarizing current in NAcC-projecting PNs in the PL cortex. *Left*, representative traces before (black) and after (grey) bath application of 20 μM DHPG. *Right*, mean number of spikes (Control, 10.92 ± 0.74; DHPG, 9.25 ± 1.08, n = 12; p = 0.059). **(B)** Effects of DHPG plus quinpirole (10 μM) with or without riluzole (5 μM) on the number of spikes. *Left*, representative traces for 100 pA-induced spikes in the control conditions (orange) and after bath application of DHPG (*D*) plus quinpirole (*Q*) without and with riluzole (*R*) (brown and dark green, respectively). *Right*, mean number of spikes (Control, 13.82 ± 1.77; + D/Q, 16.27 ± 2.05; + D/Q/R, 4.64 ± 0.87, n = 11; control vs + D/Q, $p < 0.01$; + D/Q vs +D/Q/R, $p < 0.001$). **(C-E)** Representative traces for the persistent activity elicited after the end of 100 pA depolarization current injection in the presence of DHPG alone (C), DHPG plus quinpirole (D), and DHPG/ quinpirole plus riluzole (E). The membrane potential was held at −60 mV. **(F-H)** Histograms for the duration of the persistent activity in the presence of DHPG alone (*F*, total of 48 trials in 12 cells), DHPG plus quinpirole (*G*, 44 trials in 11 cells), and DHPG/ quinpirole plus riluzole (*H*, 44 trials in 11 cells). **(I-M)**

Cocaine increases the activity of NAcC-projecting D2-PNs (I) Schematic for injections of CTB-647 into the NAcC for retrograde tracing and injection of AAV-DIO-EYFP into the PL for labeling of D2-PNs in Drd2-cre mice. (J) Experimental protocol. Saline or cocaine was injected intraperitoneally once a day for five consecutive days. After injection, the mice were allowed to freely move in the open-field for 10 min. On day 5, 2 hours after intraperitoneally injection, cardiac perfusion was performed for immunohistochemistry. (K) Confocal images showing c-fos expression in NAcC-projecting D2-PNs in the saline- (*upper*) and cocaine- (*lower*) injected animals. Arrows indicate a subset of neurons co-labeled with EYFP (green) and CTB647 (gray). Asterisks in the merged images indicate c-fos (red) labeled neurons among the cells indicated by arrows. (L) Proportions of c-fos(+) neurons among NAcC-projecting D2-PNs in saline- (*upper*) and cocaine- (*lower*) injected mice. (M) Percentages of c-fos(+) NAcC-projecting D2-PNs in individual mice (*open circles*) and their mean (*bar graph*) (Saline, 26.58 ± 1.5 %, n = 5; Cocaine, 46.93 ± 3.7 %, n = 8, $p < 0.01$). Data are shown as mean ± SEM. **$p < 0.01$, ***$p < 0.001$

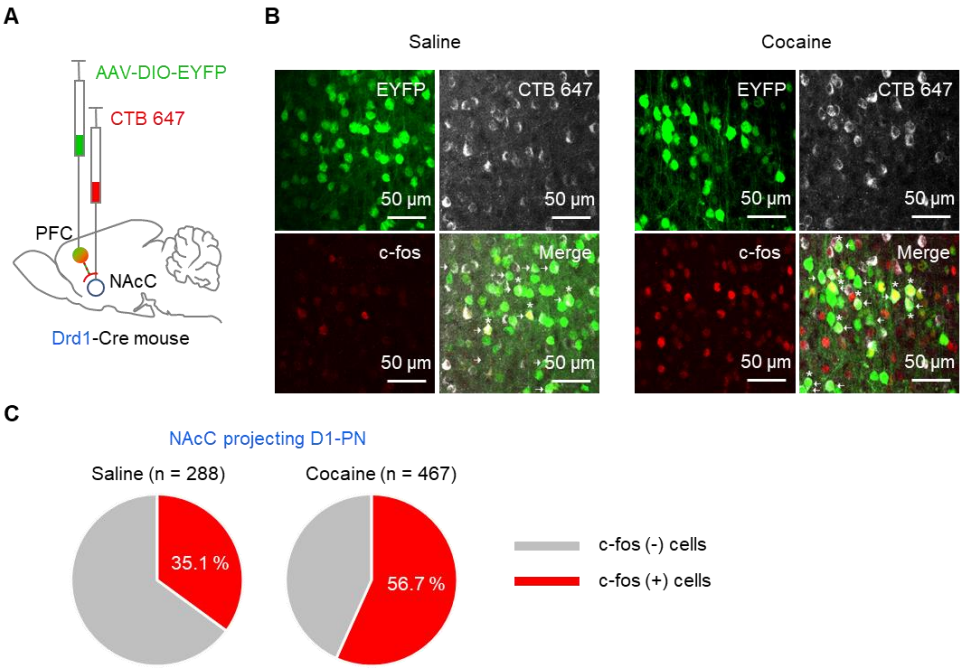
A
AAV-DIO-EYFP
CTB 647
PFC
NAcC
Drd1-Cre mouse
B
Saline
Cocaine
EYFP
CTB 647
c-fos
Merge
50 μm
C
NAcC projecting D1-PN
Saline (n = 288)
Cocaine (n = 467)
35.1 %
56.7 %
c-fos (-) cells
c-fos (+) cells

Figure 13. Cocaine increases the activity of NAcC-projecting D1-PNs. **(A)** Schematic for injections of CTB-647 into the NAcC for retrograde tracing and injection of AAV-DIO-EYFP into the PL for labeling of D1-PNs in Drd1-cre mice. **(B)** Confocal images showing c-fos expression in NAcC-projecting D1-PNs in the saline- (*left*) and cocaine- (*right*) injected animals. Arrows indicate a subset of neurons co-labeled with EYFP (green) and CTB647 (gray). Asterisks in the merged images indicate a c-fos (red) labeled neurons among the cells indicated by arrows. **(C)** Proportions of c-fos(+) neurons among NAcC-projecting D1-PNs in saline- (*left*) and cocaine- (*right*) injected mice (three mice for each group).

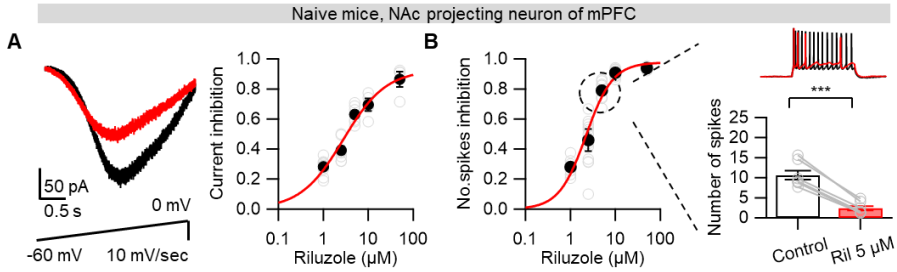
Naive mice, NAc projecting neuron of mPFC
A
50 pA
0.5 s
0 mV
-60 mV
10 mV/sec
Current inhibition
Riluzole (μM)
B
No.spikes inhibition
Riluzole (μM)
***
Number of spikes
Control
Ril 5 μM

Figure 14. Riluzole decreases the persistent Na^+ current ($I_{Na,P}$) and intrinsic excitability of PL L5 NAc-projecting PNs in naïve mice.

(A) Dose-response relationship of riluzole's effect on $I_{Na,P}$. *Left*, representative traces of $I_{Na,P}$ evoked by applying a slow voltage ramp pulse before (black) and after (red) bath application of 2.5 μM riluzole. *Right*, fraction of $I_{Na,P}$ inhibited by riluzole at different concentrations (1 μM = 0.28 ± 0.02, n = 9; 2.5 μM = 0.39 ± 0.03, n = 8; 5 μM = 0.63 ± 0.02, n = 7; 10 μM = 0.7 ± 0.04, n = 4; 50 μM = 0.87 ± 0.05, n = 4; IC_{50} = 2.21 μM) **(B)** Dose-response relationship of riluzole's effect on the number of spikes. *Left*, riluzole-induced fractional decreases of spike numbers (1 μM = 0.28 ± 0.02, n = 7; 2.5 μM = 0.46 ± 0.07, n = 12; 5 μM = 0.79 ± 0.03, n = 7; 10 μM = 0.91 ± 0.01, n = 7; 50 μM = 0.94 ± 0.01, n = 3; IC_{50} = 2.79 μM). *Right upper*, representative spike responses elicited by 100 pA injection before (black) and after (red) bath application of 5 μM riluzole. *Right lower*, summary of the spike numbers before (10.64 ± 1.1) and after applying 5 μM riluzole (2.4 ± 0.52, n = 7, $p < 0.001$). Data are shown as mean ± SEM. ***$p < 0.001$

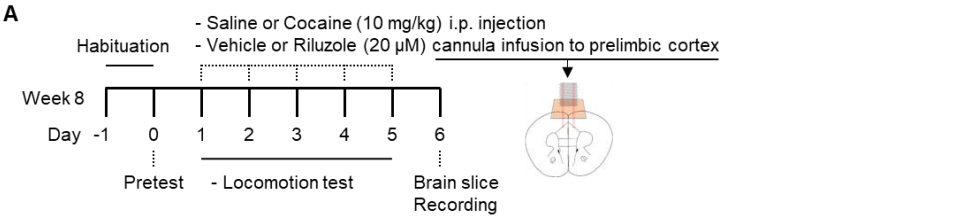

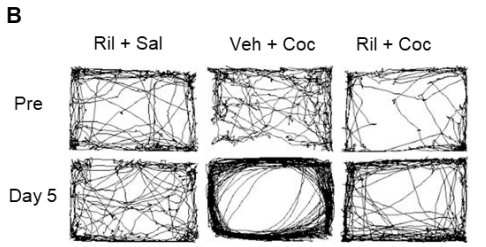

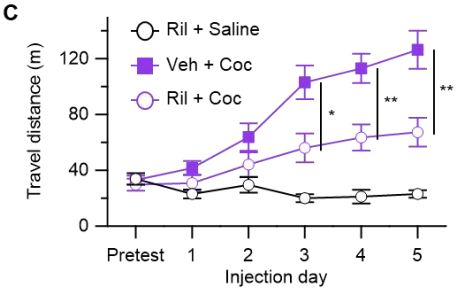

Riluzole i.p. injection (Locomotion & Conditioned Place Preference Test)

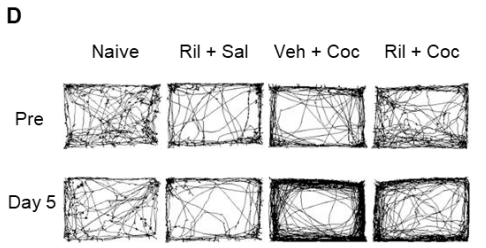

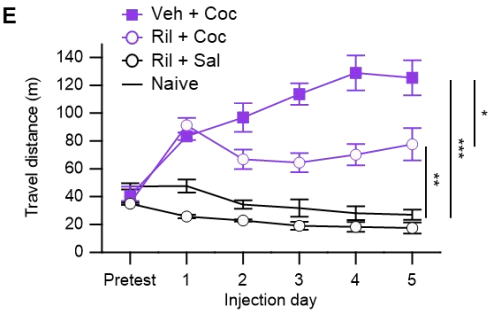

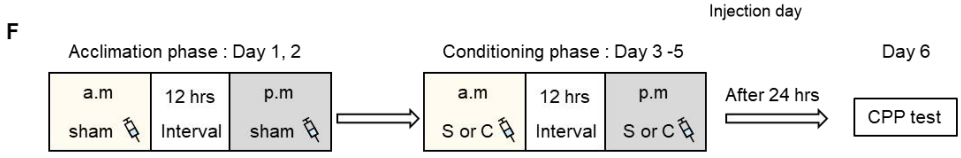

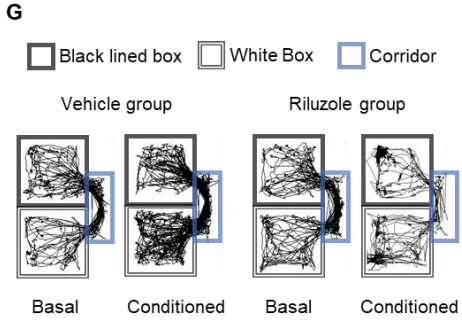

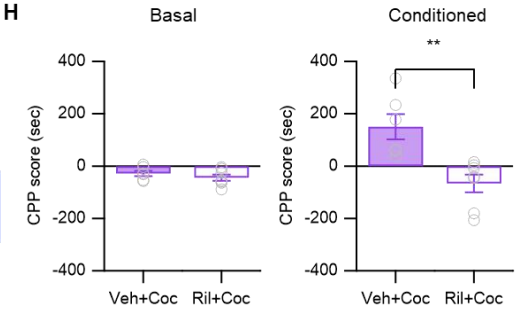

Figure 15. Riluzole prevents cocaine-induced behavioral alteration. **(A)** Experimental protocol. Vehicle (*Veh*) or riluzole (*Ril*) was infused into the PL cortex 10 min before i.p. injection of saline (*Sal*) or cocaine (*Coc*), with the animal locomotor activity test. **(B)** Representative locomotion traces before and on day 5 of riluzole or vehicle infusion 10 min before saline or cocaine i.p. injection. **(C)** Local infusion of riluzole into the PL cortex of cocaine-treated mice alleviated the locomotor sensitization. Summary for travel distance (*Ril+Sal*, Pretest, 29.95 ± 3.79 m; Day 5, 22.89 ± 1.86 m; $F_{(5,25)}$ = 1.71, p = 0.17, one-way repeated measure ANOVA; *Veh+Coc vs. Ril+Coc*, Days x Treatment: $F_{(2, 17.8)}$ = 7.25, p < 0.01; post-hoc T-test: day1, p = 0.21; day2, p = 0.17; day3, p < 0.05; day4, p < 0.01; day5, p < 0.01, two-way repeated measure ANOVA and Bonferroni's post hoc test). **(D)** Representative locomotion trace of mice treated with i.p. injections of riluzole or saline 30 min before saline or cocaine injection. **(E)** Summary for travel distance. One-way ANOVA was used to examine the differences in travel distance on day 5 [$F_{(3,9)}$ = 35.4, p < 0.001]. Compared to naive mice (26.97 ± 3.58 m, n = 4), the "vehicle + cocaine" group displayed locomotor sensitization (*Veh+Coc* ,125.39 ± 12.5 m, n = 3, p < 0.001). Whereas the "riluzole + cocaine" treatment induced locomotor sensitization (*Ril+Coc*, 77.6 ± 11.61 m, n = 3, p

< 0.01), riluzole significantly alleviated the cocaine-induced locomotor sensitization (*Veh+Coc*, 125.39 ± 12.5 m, n = 3; *Ril+Coc*, 77.6 ± 11.61 m, n = 3; p < 0.05). Riluzole i.p. injection did not affect basal locomotion (*Ril+Sal*, 17.49 ± 3.96 m, n = 3, p = 0.84). Tukey's post hoc multiple comparisons test was used for group differences determination. **(F)** Experimental scheme for cocaine-conditioned place preference (CPP) test. **(G)** Representative track of mice. *Left* in each group shows basal preference recording and *right* in each group shows CPP test recording. **(H)** Summary bar graphs of CPP scores. There was no significant difference in basal preference between the "vehicle + cocaine" and "riluzole + cocaine" groups (*Left*, veh+coc, −27.97 ± 10.31 sec, n= 6; ril+coc, −44.11 ± 11.73 sec, n = 7, p = 0.3), while riluzole significantly alleviated the cocaine-induced place preference (*Right*, veh+coc, 150.6 ± 48.51 sec, n= 6; ril+coc, −66.24 ± 34.08 sec, n = 7, p < 0.01). Data are shown as mean ± SEM. *p < 0.05, **p < 0.01. ***p <0.001

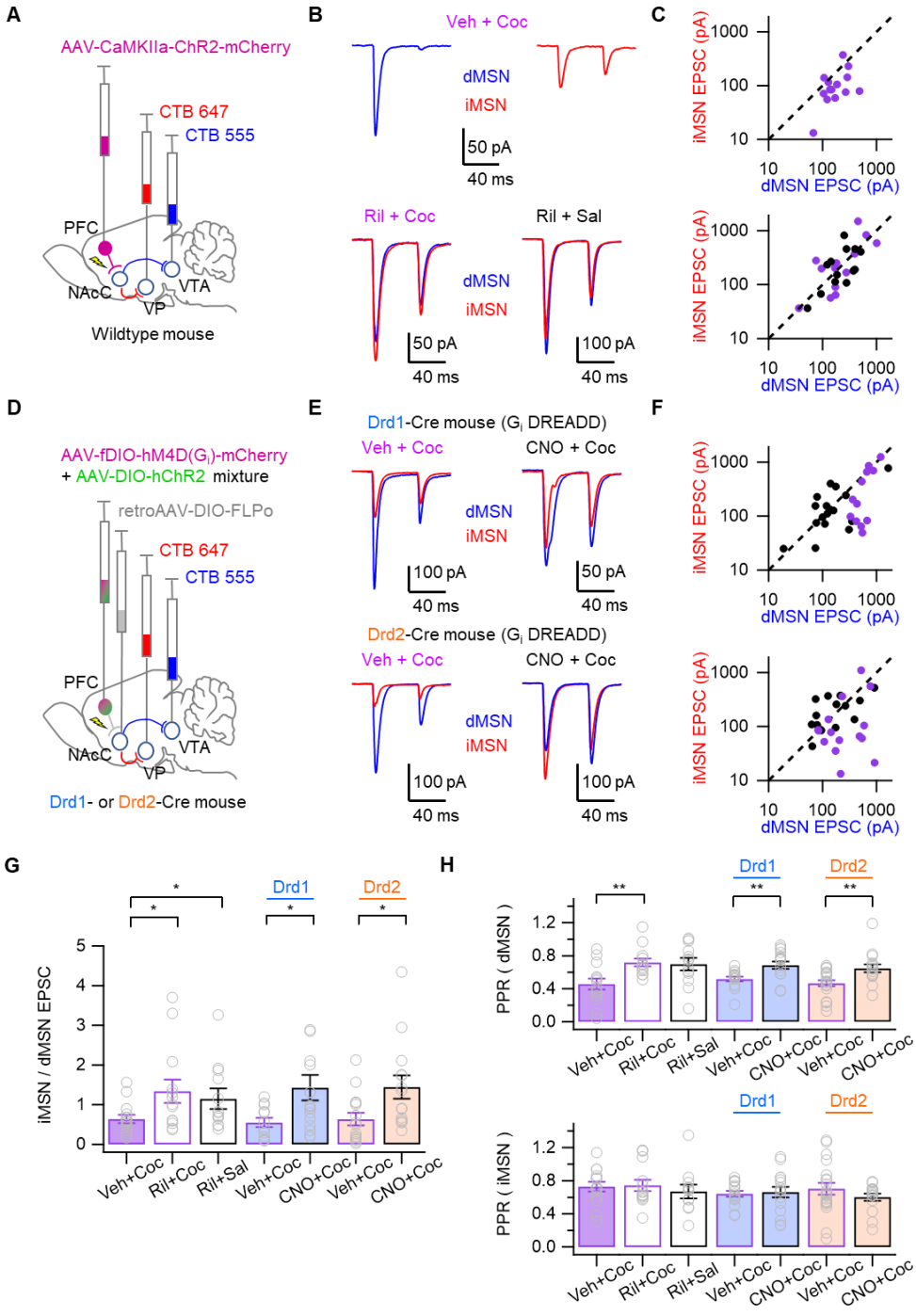
A
AAV-CaMKIIa-ChR2-mCherry
CTB 647
CTB 555
PFC
NAcC
VTA
VP
Wildtype mouse
B
Veh + Coc
dMSN
iMSN
50 pA
40 ms
Ril + Coc
Ril + Sal
50 pA
100 pA
40 ms
C
iMSN EPSC (pA)
dMSN EPSC (pA)
1000
100
10
D
AAV-fDIO-hM4D(Gi)-mCherry
+ AAV-DIO-hChR2 mixture
retroAAV-DIO-FLPo
CTB 647
CTB 555
PFC
NAcC
VTA
VP
Drd1- or Drd2-Cre mouse
E
Drd1-Cre mouse (Gi DREADD)
Veh + Coc
CNO + Coc
dMSN
iMSN
100 pA
50 pA
40 ms
Drd2-Cre mouse (Gi DREADD)
F
G
iMSN / dMSN EPSC
Drd1
Drd2
Veh+Coc
Ril+Coc
Ril+Sal
CNO+Coc
H
PPR (dMSN)
PPR (iMSN)

Figure 16. Reduced intrinsic excitability of PN in the PL cortex prevents cocaine induced synaptic change.

(A) Schematic for the retrograde labeling of the MSNs and the expression of ChR2 in PL neurons. For retrograde labeling of iMSNs and dMSNs, CTB-647 (red) and CTB-555 (blue) were injected into VP and VTA, respectively. For selective opto-stimulation, AAV-CaMKIIa-ChR2 was injected into the PL cortex of wildtype mice. **(B)** Representative trace of PL axon stimulation-evoked EPSCs recorded in neighboring dMSNs (blue) and iMSNs (red). *Upper row*, mice treated with "vehicle + cocaine". *Lower row*, "riluzole + cocaine" group and "riluzole + saline" group. **(C)** plot of iMSN- *vs.* dMSN-EPSC amplitudes (log scale). *Upper row*, mice treated with "vehicle + cocaine". *Lower row*, "riluzole + cocaine" group and "riluzole + saline" group. **(D)** Schematic for the retrograde labling of the MSNs and the expression of ChR2 and hM4D(G_i) in PL neurons. For retrograde labeling of iMSNs and dMSNs, CTB-647 and CTB-555 were injected into VP and VTA, respectively. Mixture of AAV-DIO-hChR2 and AAV-fDIO-hM4D(G_i)-mCherry was injected into the PL and retroAAV-DIO-FLPo was injected into the NAcC of D1- or D2-cre mice for selective opto-stimulation of D1- or D2-PNs and targeting the CNO action to NAcC-projecting neurons. Chemogenetic reduction

of excitability of D1- (upper row) and D2-PNs (lower row) prevents cocaine-induced rewiring. **(E)** Representative trace of PL axon stimulation-evoked EPSCs recorded in neighboring dMSNs (blue) and iMSNs (red). **(F)** plot of iMSN- vs dMSN-EPSC amplitudes (log scale). Magenta symbols represent "vehicle + cocaine" group and black symbols represent "CNO + cocaine" group. **(G)** iMSN/dMSN EPSC amplitude ratio (WT mouse, *Veh+Coc*, 0.64 ± 0.11, n = 14; *Ril+Coc*, 1.34 ± 0.3, n = 13; *Ril+Sal*, 1.15 ± 0.26, n = 13;Drd1 mouse, *Veh+Coc*, 0.55 ± 0.11, n = 12; *CNO+Coc*, 1.18 ± 0.21, n = 16; Drd2 mouse, *Veh+Coc*, 0.63 ± 0.16, n = 15; *CNO+Coc*, 1.44 ± 0.3, n = 14; WT mouse, *Veh+Coc vs. Ril+Coc*, $p < 0.05$; *Veh+Coc vs. Ril+Sal*, $p < 0.05$; *Ril+Coc vs. Ril+Sal*, $p = 0.74$; Drd1 mouse, *Veh+Coc vs. CNO+Coc*, $p < 0.05$; Drd2 mouse, *Veh+Coc vs. CNO+Coc*, $p < 0.05$). **(H)** Summary of PPR. *Upper*, PPRs of dMSN-EPSCs (WT mouse, *Veh+Coc*, 0.46 ± 0.06, n = 14; *Ril+Coc*, 0.72 ± 0.05, n = 13; *Ril+Sal*, 0.7 ± 0.08, n = 13; Drd1 mouse, *Veh+Coc*, 0.52 ± 0.03, n = 15; *CNO+Coc*, 0.69 ± 0.05, n = 16; Drd2 mouse, *Veh+Coc*, 0.47 ± 0.04, n = 20; *CNO+Coc*, 0.65 ± 0.05, n = 16; WT mouse, *Veh+Coc vs. Ril+Coc*, $p < 0.01$; *Veh+Coc vs. Ril+Sal*, $p < 0.05$; *Ril+Coc vs. Ril+Sal*, $p = 0.94$; Drd1 mouse, *Veh+Coc vs CNO+Coc*, $p < 0.01$; Drd2 mouse, *Veh+Coc vs CNO+Coc*, $p < 0.01$). *Lower*, PPRs of iMSN-EPSCs

(WT mouse, *Veh+Coc*, 0.73 ± 0.06, n = 14; *Ril+Coc*, 0.74 ± 0.07, n = 13; *Ril+Sal*, 0.67 ± 0.08, n = 13; Drd1 mouse, *Veh+Coc*, 0.64 ± 0.03, n = 16; *CNO+Coc*, 0.66 ± 0.06, n = 16; Drd2 mouse, *Veh+Coc*, 0.7 ± 0.07, n = 20; *CNO+Coc*, 0.6 ± 0.04, n = 15; WT mouse, *Veh+Coc vs. Ril+Coc*, p = 0.73; *Veh+Coc vs. Ril+Sal*, p = 0.3; *Ril+Coc vs. Ril+Sal*, p = 0.47 ; Drd1 mouse, *Veh+Coc vs. CNO+Coc*, p = 0.65; Drd2 mouse, *Veh+Coc vs. CNO+Coc*, p = 0.59). $^{*}p < 0.05$, $^{**}p < 0.01$. Data are shown as mean ± SEM.

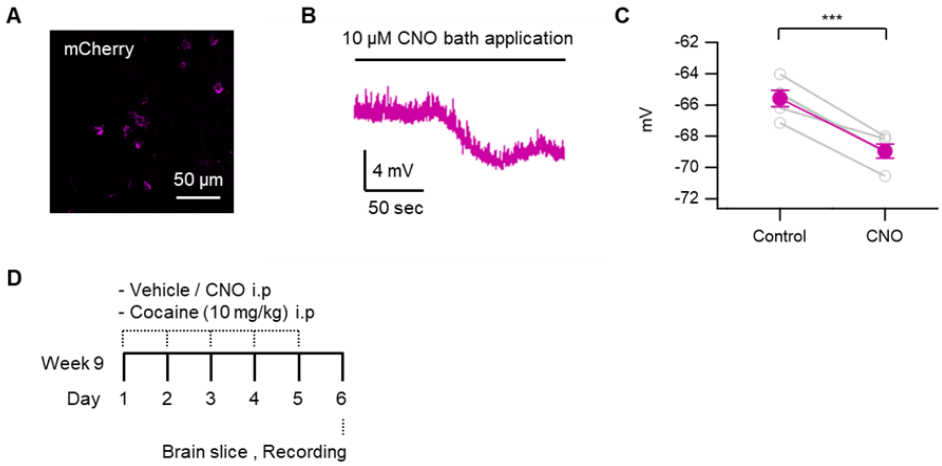
A
mCherry
50 μm
B
10 μM CNO bath application
4 mV
50 sec
C
***
-62
-64
-66
-68
-70
-72
mV
Control
CNO
D
- Vehicle / CNO i.p
- Cocaine (10 mg/kg) i.p
Week 9
Day 1 2 3 4 5 6
Brain slice , Recording

Figure 17. Experimental protocol for Figure 7E–H, and validation for hM4D(G_i) expression in NAcC–projecting PNs in the PL

(A) Confocal images of mCherry labeled NAcC–projecting neurons. **(B)** Representative trace of membrane potential change during 10 μM CNO bath application. **(C)** Summary of the membrane potential before (−65.28 ± 0.77 mV) and after applying 10 μM CNO (−69.02 ± 0.62 mV, n = 5, $p < 0.001$). **(D)** Schematic of the cocaine sensitization protocol for performing figure 6E–G experiments. Cocaine was injected intraperitoneally 30 min after i.p injection of vehicle or CNO for five consecutive days. On day 6, brain slices were obtained for electrophysiological recording. Representative trace of membrane potential change during 10 μM CNO bath application. Data are shown as mean ± SEM. ***$p < 0.001$

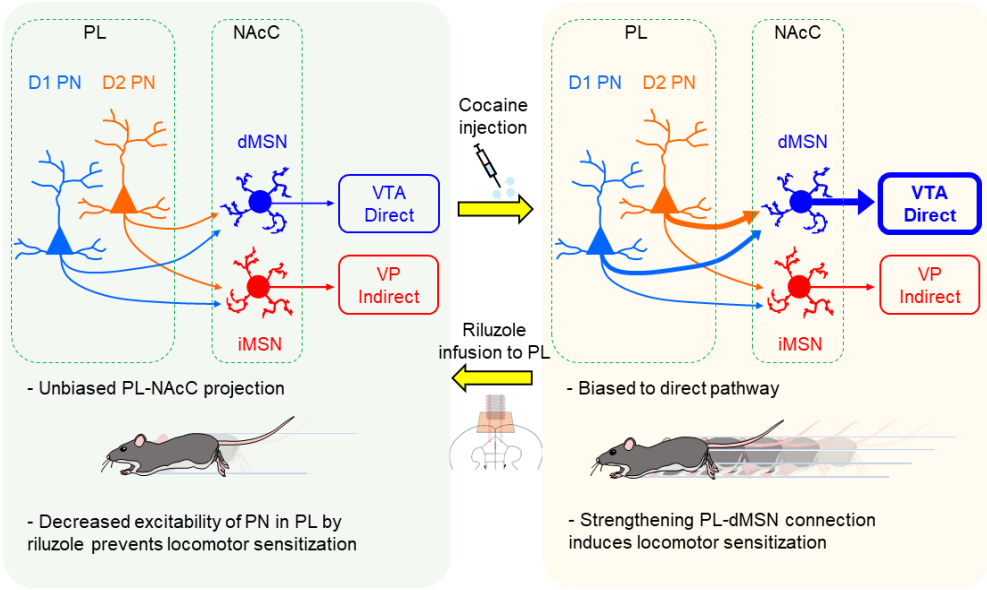
PL
NAcC
D1 PN
D2 PN
dMSN
iMSN
VTA
Direct
VP
Indirect
Cocaine
injection
Riluzole
infusion to PL
- Unbiased PL-NAcC projection
- Decreased excitability of PN in PL by riluzole prevents locomotor sensitization
- Biased to direct pathway
- Strengthening PL-dMSN connection induces locomotor sensitization

Figure 18. Schematic models for cocaine-induced rewiring of PL-to-NAcC synapses underlying cocaine sensitization.

Repeated cocaine injections bias the connection toward the direct pathway. The rewired pathway induces LS, but riluzole infusion to the PL cortex reduced LS by preventing rewiring.

References

Anastasiades, P. G., J. J. Marlin and A. G. Carter (2018). "Cell-Type Specificity of Callosally Evoked Excitation and Feedforward Inhibition in the Prefrontal Cortex." Cell Rep 22(3): 679-692.

Arancio, O., M. Kiebler, C. J. Lee, V. Lev-Ram, R. Y. Tsien, E. R. Kandel and R. D. Hawkins (1996). "Nitric oxide acts directly in the presynaptic neuron to produce long-term potentiation in cultured hippocampal neurons." Cell 87(6): 1025-1035.

Avesar, D. and A. T. Gulledge (2012). "Selective serotonergic excitation of callosal projection neurons." Front Neural Circuits 6: 12.

Bae, J. W., H. Jeong, Y. J. Yoon, C. M. Bae, H. Lee, S. B. Paik and M. W. Jung (2021). "Parallel processing of working memory and temporal information by distinct types of cortical projection neurons." Nat Commun 12(1): 4352.

Baimel, C., L. M. McGarry and A. G. Carter (2019). "The Projection Targets of Medium Spiny Neurons Govern Cocaine-Evoked Synaptic Plasticity in the Nucleus Accumbens." Cell Rep 28(9): 2256-2263 e2253.

Baker, A., B. Kalmbach, M. Morishima, J. Kim, A. Juavinett, N. Li and N. Dembrow (2018). "Specialized Subpopulations of Deep-Layer Pyramidal Neurons in the Neocortex: Bridging Cellular Properties to Functional Consequences." J Neurosci 38(24): 5441-5455.

Bellingham, M. C. (2011). "A review of the neural mechanisms of action and clinical efficiency of riluzole in treating amyotrophic lateral sclerosis: what have we learned in the last decade?" CNS Neurosci Ther 17(1): 4-31.

Beltramo, R., G. D'Urso, M. Dal Maschio, P. Farisello, S. Bovetti, Y. Clovis, G. Lassi, V. Tucci, D. De Pietri Tonelli and T. Fellin (2013). "Layer-specific excitatory circuits differentially control recurrent network dynamics in the neocortex." Nat Neurosci 16(2): 227-234.

Bensimon, G., L. Lacomblez and V. Meininger (1994). "A controlled trial of riluzole in amyotrophic lateral sclerosis. ALS/Riluzole Study Group." N Engl J Med 330(9): 585-591.

Bock, R., J. H. Shin, A. R. Kaplan, A. Dobi, E. Markey, P. F. Kramer, C. M. Gremel, C. H. Christensen, M. F. Adrover and V. A. Alvarez (2013). "Strengthening the accumbal indirect pathway promotes resilience to compulsive cocaine use." Nat Neurosci 16(5): 632-638.

Bocklisch, C., V. Pascoli, J. C. Wong, D. R. House, C. Yvon, M. de Roo, K. R. Tan and C. Luscher (2013). "Cocaine disinhibits dopamine neurons by potentiation of GABA transmission in the ventral tegmental area." Science 341(6153): 1521-1525.

Brog, J. S., A. Salyapongse, A. Y. Deutch and D. S. Zahm (1993). "The patterns of afferent innervation of the core and shell in the "accumbens" part of the rat ventral striatum: immunohistochemical detection of retrogradely transported fluoro-gold." J Comp Neurol 338(2): 255-278.

Chen, L., J. D. Bohanick, M. Nishihara, J. K. Seamans and C. R. Yang (2007). "Dopamine D1/5 receptor-mediated long-term potentiation of intrinsic excitability in rat prefrontal cortical neurons: Ca2+-dependent intracellular signaling." J Neurophysiol 97(3): 2448-2464.

Chiamulera, C., M. P. Epping-Jordan, A. Zocchi, C. Marcon, C. Cottiny, S. Tacconi, M. Corsi, F. Orzi and F. Conquet (2001). "Reinforcing and locomotor stimulant effects of cocaine are absent in mGluR5 null mutant mice." Nat Neurosci 4(9): 873-874.

Cools, R. and A. F. T. Arnsten (2022). "Neuromodulation of prefrontal cortex cognitive function in primates: the powerful roles of monoamines and acetylcholine." Neuropsychopharmacology 47(1): 309-328.

Crill, W. E. (1996). "Persistent sodium current in mammalian central neurons." Annu Rev Physiol 58: 349-362.

Cui, Y., V. Paille, H. Xu, S. Genet, B. Delord, E. Fino, H. Berry and L. Venance (2015). "Endocannabinoids mediate bidirectional striatal spike-timing-dependent plasticity." J Physiol 593(13): 2833-2849.

Cummings, K. A. and R. L. Clem (2020). "Prefrontal somatostatin interneurons encode fear memory." Nat Neurosci 23(1): 61-74.

Curtis, C. E. and M. D'Esposito (2003). "Persistent activity in the prefrontal cortex during working memory." Trends Cogn Sci 7(9): 415-423.

Dembrow, N. C., R. A. Chitwood and D. Johnston (2010). "Projection-specific neuromodulation of medial prefrontal cortex neurons." J Neurosci 30(50): 16922-16937.

Deroche, M. A., O. Lassalle, L. Castell, E. Valjent and O. J. Manzoni (2020). "Cell-Type- and Endocannabinoid-Specific Synapse Connectivity in the Adult Nucleus Accumbens Core." J Neurosci 40(5): 1028-1041.

Di Ciano, P. and B. J. Everitt (2001). "Dissociable effects of antagonism of NMDA and AMPA/KA receptors in the nucleus accumbens core and shell on cocaine-seeking behavior." Neuropsychopharmacology 25(3): 341-360.

Dong, Y., F. J. Nasif, J. J. Tsui, W. Y. Ju, D. C. Cooper, X. T. Hu, R. C. Malenka and F. J. White (2005). "Cocaine-induced plasticity of intrinsic membrane properties in prefrontal cortex pyramidal neurons: adaptations in potassium currents." J Neurosci 25(4): 936-940.

Durieux, P. F., B. Bearzatto, S. Guiducci, T. Buch, A. Waisman, M. Zoli, S. N. Schiffmann and A. de Kerchove d'Exaerde (2009). "D2R striatopallidal neurons inhibit both locomotor and drug reward processes." Nat Neurosci 12(4): 393-395.

Gee, S., I. Ellwood, T. Patel, F. Luongo, K. Deisseroth and V. S. Sohal (2012). "Synaptic activity unmasks dopamine D2 receptor modulation of a specific class of layer V pyramidal neurons in prefrontal cortex." J Neurosci 32(14): 4959-4971.

Gerfen, C. R., M. N. Economo and J. Chandrashekar (2018). "Long distance projections of cortical pyramidal neurons." J Neurosci Res 96(9): 1467-1475.

Gerfen, C. R., R. Paletzki and N. Heintz (2013). "GENSAT BAC cre-recombinase driver lines to study the functional organization of cerebral cortical and basal ganglia circuits." Neuron 80(6): 1368-1383.

Gill, T. M., P. J. Castaneda and P. H. Janak (2010). "Dissociable roles of the medial prefrontal cortex and nucleus accumbens core in

goal-directed actions for differential reward magnitude." Cereb Cortex 20(12): 2884-2899.

Grueter, B. A., G. Brasnjo and R. C. Malenka (2010). "Postsynaptic TRPV1 triggers cell type-specific long-term depression in the nucleus accumbens." Nat Neurosci 13(12): 1519-1525.

Gulledge, A. T. and D. B. Jaffe (1998). "Dopamine decreases the excitability of layer V pyramidal cells in the rat prefrontal cortex." J Neurosci 18(21): 9139-9151.

Harris, K. D. and G. M. Shepherd (2015). "The neocortical circuit: themes and variations." Nat Neurosci 18(2): 170-181.

Heimer, L., D. S. Zahm, L. Churchill, P. W. Kalivas and C. Wohltmann (1991). "Specificity in the projection patterns of accumbal core and shell in the rat." Neuroscience 41(1): 89-125.

Hernandez-Lopez, S., T. Tkatch, E. Perez-Garci, E. Galarraga, J. Bargas, H. Hamm and D. J. Surmeier (2000). "D2 dopamine receptors in striatal medium spiny neurons reduce L-type Ca2+ currents and excitability via a novel PLC[beta]1-IP3-calcineurin-signaling cascade." J Neurosci 20(24): 8987-8995.

Hikida, T., K. Kimura, N. Wada, K. Funabiki and S. Nakanishi (2010). "Distinct roles of synaptic transmission in direct and indirect striatal pathways to reward and aversive behavior." Neuron 66(6): 896-907.

Hikida, T., S. Yawata, T. Yamaguchi, T. Danjo, T. Sasaoka, Y. Wang and S. Nakanishi (2013). "Pathway-specific modulation of nucleus accumbens in reward and aversive behavior via selective transmitter receptors." Proc Natl Acad Sci U S A 110(1): 342-347.

Huang, Z. J. (2014). "Toward a genetic dissection of cortical circuits in the mouse." Neuron 83(6): 1284-1302.

Hyman, S. E., R. C. Malenka and E. J. Nestler (2006). "Neural mechanisms of addiction: the role of reward-related learning and memory." Annu Rev Neurosci 29: 565-598.

Jones, E. G. and A. Peters (1990). Comparative structure and evolution of cerebral cortex, Plenum.

Kalivas, P. W., R. T. Lalumiere, L. Knackstedt and H. Shen (2009). "Glutamate transmission in addiction." Neuropharmacology 56 Suppl 1: 169-173.

Kalmbach, B. E., R. A. Chitwood, N. C. Dembrow and D. Johnston (2013). "Dendritic generation of mGluR-mediated slow afterdepolarization in layer 5 neurons of prefrontal cortex." J Neurosci 33(33): 13518-13532.

Katz, E., O. Stoler, A. Scheller, Y. Khrapunsky, S. Goebbels, F. Kirchhoff, M. J. Gutnick, F. Wolf and I. A. Fleidervish (2018). "Role of sodium channel subtype in action potential generation by

neocortical pyramidal neurons." Proc Natl Acad Sci U S A 115(30): E7184-E7192.

Kawahara, Y., Y. N. Ohnishi, Y. H. Ohnishi, H. Kawahara and A. Nishi (2021). "Distinct Role of Dopamine in the PFC and NAc During Exposure to Cocaine-Associated Cues." Int J Neuropsychopharmacol 24(12): 988-1001.

Koch, W. J., B. E. Hawes, L. F. Allen and R. J. Lefkowitz (1994). "Direct evidence that Gi-coupled receptor stimulation of mitogen-activated protein kinase is mediated by G beta gamma activation of p21ras." Proc Natl Acad Sci U S A 91(26): 12706-12710.

Kravitz, A. V., L. D. Tye and A. C. Kreitzer (2012). "Distinct roles for direct and indirect pathway striatal neurons in reinforcement." Nat Neurosci 15(6): 816-818.

Kupchik, Y. M., R. M. Brown, J. A. Heinsbroek, M. K. Lobo, D. J. Schwartz and P. W. Kalivas (2015). "Coding the direct/indirect pathways by D1 and D2 receptors is not valid for accumbens projections." Nat Neurosci 18(9): 1230-1232.

Lampl, I., P. Schwindt and W. Crill (1998). "Reduction of cortical pyramidal neuron excitability by the action of phenytoin on persistent Na+ current." J Pharmacol Exp Ther 284(1): 228-237.

Le Bon-Jego, M. and R. Yuste (2007). "Persistently active, pacemaker-like neurons in neocortex." Front Neurosci 1(1): 123-129.

Liu, W. Z., W. H. Zhang, Z. H. Zheng, J. X. Zou, X. X. Liu, S. H. Huang, W. J. You, Y. He, J. Y. Zhang, X. D. Wang and B. X. Pan (2020). "Identification of a prefrontal cortex-to-amygdala pathway for chronic stress-induced anxiety." Nat Commun 11(1): 2221.

Liu, Z., Q. Le, Y. Lv, X. Chen, J. Cui, Y. Zhou, D. Cheng, C. Ma, X. Su, L. Xiao, R. Yang, J. Zhang, L. Ma and X. Liu (2022). "A distinct D1-MSN subpopulation down-regulates dopamine to promote negative emotional state." Cell Res 32(2): 139-156.

MacAskill, A. F., J. M. Cassel and A. G. Carter (2014). "Cocaine exposure reorganizes cell type- and input-specific connectivity in the nucleus accumbens." Nat Neurosci 17(9): 1198-1207.

Molnar, Z. and A. F. Cheung (2006). "Towards the classification of subpopulations of layer V pyramidal projection neurons." Neurosci Res 55(2): 105-115.

Morishima, M. and Y. Kawaguchi (2006). "Recurrent connection patterns of corticostriatal pyramidal cells in frontal cortex." J Neurosci 26(16): 4394-4405.

Murthy, K. S., D. H. Coy and G. M. Makhlouf (1996). "Somatostatin receptor-mediated signaling in smooth muscle. Activation of

phospholipase C-beta3 by Gbetagamma and inhibition of adenylyl cyclase by Galphai1 and Galphao." J Biol Chem 271(38): 23458-23463.

Murthy, K. S., H. Zhou, J. Huang and S. N. Pentyala (2004). "Activation of PLC-delta1 by Gi/o-coupled receptor agonists." Am J Physiol Cell Physiol 287(6): C1679-1687.

Narayanan, R. T., D. Udvary and M. Oberlaender (2017). "Cell Type-Specific Structural Organization of the Six Layers in Rat Barrel Cortex." Front Neuroanat 11: 91.

Oswald, M. J., M. L. Tantirigama, I. Sonntag, S. M. Hughes and R. M. Empson (2013). "Diversity of layer 5 projection neurons in the mouse motor cortex." Front Cell Neurosci 7: 174.

Otis, J. M., K. B. Dashew and D. Mueller (2013). "Neurobiological dissociation of retrieval and reconsolidation of cocaine-associated memory." J Neurosci 33(3): 1271-1281a.

Pascoli, V., M. Turiault and C. Luscher (2012). "Reversal of cocaine-evoked synaptic potentiation resets drug-induced adaptive behaviour." Nature 481(7379): 71-75.

Philip, F., G. Kadamur, R. G. Silos, J. Woodson and E. M. Ross (2010). "Synergistic activation of phospholipase C-beta3 by Galpha(q) and Gbetagamma describes a simple two-state coincidence detector." Curr Biol 20(15): 1327-1335.

Pierce, R. C., D. C. Reeder, J. Hicks, Z. R. Morgan and P. W. Kalivas (1998). "Ibotenic acid lesions of the dorsal prefrontal cortex disrupt the expression of behavioral sensitization to cocaine." Neuroscience 82(4): 1103-1114.

Pieri, M., I. Carunchio, L. Curcio, N. B. Mercuri and C. Zona (2009). "Increased persistent sodium current determines cortical hyperexcitability in a genetic model of amyotrophic lateral sclerosis." Exp Neurol 215(2): 368-379.

Popescu, I. R., K. Q. Le, R. Palenzuela, R. Voglewede and R. Mostany (2017). "Marked bias towards spontaneous synaptic inhibition distinguishes non-adapting from adapting layer 5 pyramidal neurons in the barrel cortex." Sci Rep 7(1): 14959.

Radnikow, G. and D. Feldmeyer (2018). "Layer- and Cell Type-Specific Modulation of Excitatory Neuronal Activity in the Neocortex." Front Neuroanat 12: 1.

Reiner, A., Y. Jiao, N. Del Mar, A. V. Laverghetta and W. L. Lei (2003). "Differential morphology of pyramidal tract-type and intratelencephalically projecting-type corticostriatal neurons and their intrastriatal terminals in rats." J Comp Neurol 457(4): 420-440.

Rhee, S. G. (2001). "Regulation of phosphoinositide-specific phospholipase C." Annu Rev Biochem 70: 281-312.

Saiki, A., Y. Sakai, R. Fukabori, S. Soma, J. Yoshida, M. Kawabata, H. Yawo, K. Kobayashi, M. Kimura and Y. Isomura (2018). "In Vivo Spiking Dynamics of Intra- and Extratelencephalic Projection Neurons in Rat Motor Cortex." Cereb Cortex 28(3): 1024-1038.

Schmitt, L. I., R. D. Wimmer, M. Nakajima, M. Happ, S. Mofakham and M. M. Halassa (2017). "Thalamic amplification of cortical connectivity sustains attentional control." Nature 545(7653): 219-223.

Seong, H. J. and A. G. Carter (2012). "D1 receptor modulation of action potential firing in a subpopulation of layer 5 pyramidal neurons in the prefrontal cortex." J Neurosci 32(31): 10516-10521.

Sesack, S. R. and A. A. Grace (2010). "Cortico-Basal Ganglia reward network: microcircuitry." Neuropsychopharmacology 35(1): 27-47.

Shah, B. H., A. Siddiqui, K. A. Qureshi, M. Khan, S. Rafi, V. A. Ujan, M. Y. Yakoob, H. Rasheed and S. A. Saeed (1999). "Co-activation of Gi and Gq proteins exerts synergistic effect on human platelet aggregation through activation of phospholipase C and Ca2+ signalling pathways." Exp Mol Med 31(1): 42-46.

Sheets, P. L., B. A. Suter, T. Kiritani, C. S. Chan, D. J. Surmeier and G. M. Shepherd (2011). "Corticospinal-specific HCN expression in mouse motor cortex: I(h)-dependent synaptic integration as a

candidate microcircuit mechanism involved in motor control." J Neurophysiol 106(5): 2216-2231.

Shimamura, A. P. (2000). "The role of the prefrontal cortex in dynamic filtering." Psychobiology 28(2): 207-218.

Sidiropoulou, K., F. M. Lu, M. A. Fowler, R. Xiao, C. Phillips, E. D. Ozkan, M. X. Zhu, F. J. White and D. C. Cooper (2009). "Dopamine modulates an mGluR5-mediated depolarization underlying prefrontal persistent activity." Nat Neurosci 12(2): 190-199.

Siniscalchi, A., A. Bonci, N. B. Mercuri and G. Bernardi (1997). "Effects of riluzole on rat cortical neurones: an in vitro electrophysiological study." Br J Pharmacol 120(2): 225-230.

Smith, Y., M. D. Bevan, E. Shink and J. P. Bolam (1998). "Microcircuitry of the direct and indirect pathways of the basal ganglia." Neuroscience 86(2): 353-387.

Sorg, B. A., D. L. Davidson, P. W. Kalivas and B. M. Prasad (1997). "Repeated daily cocaine alters subsequent cocaine-induced increase of extracellular dopamine in the medial prefrontal cortex." J Pharmacol Exp Ther 281(1): 54-61.

Steketee, J. D. and P. W. Kalivas (2011). "Drug wanting: behavioral sensitization and relapse to drug-seeking behavior." Pharmacol Rev 63(2): 348-365.

Suska, A., B. R. Lee, Y. H. Huang, Y. Dong and O. M. Schluter (2013). "Selective presynaptic enhancement of the prefrontal cortex to nucleus accumbens pathway by cocaine." Proc Natl Acad Sci U S A 110(2): 713-718.

Terra, H., B. Bruinsma, S. F. de Kloet, M. van der Roest, T. Pattij and H. D. Mansvelder (2020). "Prefrontal Cortical Projection Neurons Targeting Dorsomedial Striatum Control Behavioral Inhibition." Curr Biol 30(21): 4188-4200 e4185.

Tzschentke, T. M. (2000). "The medial prefrontal cortex as a part of the brain reward system." Amino Acids 19(1): 211-219.

Tzschentke, T. M. and W. J. Schmidt (2003). "Glutamatergic mechanisms in addiction." Mol Psychiatry 8(4): 373-382.

Urbani, A. and O. Belluzzi (2000). "Riluzole inhibits the persistent sodium current in mammalian CNS neurons." Eur J Neurosci 12(10): 3567-3574.

van Zessen, R., Y. Li, L. Marion-Poll, N. Hulo, J. Flakowski and C. Luscher (2021). "Dynamic dichotomy of accumbal population activity underlies cocaine sensitization." Elife 10.

Wang, J. and P. O'Donnell (2001). "D(1) dopamine receptors potentiate nmda-mediated excitability increase in layer V prefrontal cortical pyramidal neurons." Cereb Cortex 11(5): 452-462.

Wang, Y. and P. S. Goldman-Rakic (2004). "D2 receptor regulation of synaptic burst firing in prefrontal cortical pyramidal neurons." Proc Natl Acad Sci U S A 101(14): 5093-5098.

Williams, J. M. and J. D. Steketee (2004). "Cocaine increases medial prefrontal cortical glutamate overflow in cocaine-sensitized rats: a time course study." Eur J Neurosci 20(6): 1639-1646.

Yang, C. R. and J. K. Seamans (1996). "Dopamine D1 receptor actions in layers V-VI rat prefrontal cortex neurons in vitro: modulation of dendritic-somatic signal integration." J Neurosci 16(5): 1922-1935.

Yang, Y. and N. Calakos (2013). "Presynaptic long-term plasticity." Front Synaptic Neurosci 5: 8.

Zhang, Z., S. Cordeiro Matos, S. Jego, A. Adamantidis and P. Seguela (2013). "Norepinephrine drives persistent activity in prefrontal cortex via synergistic alpha1 and alpha2 adrenoceptors." PLoS One 8(6): e66122.

Zhou, Y., E. Yan, D. Cheng, H. Zhu, Z. Liu, X. Chen, L. Ma and X. Liu (2020). "The Projection From Ventral CA1, Not Prefrontal Cortex, to Nucleus Accumbens Core Mediates Recent Memory Retrieval of Cocaine-Conditioned Place Preference." Front Behav Neurosci 14: 558074.

Zhou, Y., H. Zhu, Z. Liu, X. Chen, X. Su, C. Ma, Z. Tian, B. Huang, E. Yan, X. Liu and L. Ma (2019). "A ventral CA1 to nucleus accumbens core engram circuit mediates conditioned place preference for cocaine." Nat Neurosci **22**(12): 1986-1999.

국 문 초 록

내측 전전두엽 피질(mPFC)은 다양한 투사 대상을 가지고 있으며, 이 대상들은 외종뇌(Extra-telencephalic, ET)영역 그룹과 내종뇌구역(Intra-telencephalic, IT)영역 그룹으로 나뉜다. mPFC의 추체뉴런(Pyramidal neuron, PN)은 투사 대상이 ET 영역 혹은 IT 영역인지에 따라 생리학적 특성이 다르다. 특히, 지속성 나트륨 전류(Persistent Na^+ current, $I_{Na,P}$)에 의존적인 지속 활성은 IT 세포보다 ET 세포에서 빈번하게 발생한다. 이와 같이 $I_{Na,P}$는 반복발화를 발생시키고 유지하는데 핵심적인 역할을 하지만, 내재적 흥분성에 대한 세포 유형별 $I_{Na,P}$의 기여에 관한 연구는 미비하다. 이에 본 연구는 역행 추적 및 패치 클램프 기술을 사용하여 ET 세포와 IT 세포 간의 전기생리학적 고유 특성과 $I_{Na,P}$의 크기를 비교하였으며, $I_{Na,P}$ 차단제인 Riluzole을 사용하여 내재적 흥분성의 변화를 확인하였다. 그 결과 ET 세포와 IT 세포는 Sag 비율, 입력 저항 및 내재적 흥분성과 같은 서로 다른 고유 특성을 가지고 있었으며, $I_{Na,P}$는 ET 세포가 IT 세포보다 더 컸다. Riluzole에 의한 $I_{Na,P}$의 감소는 ET 세포와 IT 세포 모두의 고유 흥분성을 감소시켰으나, 그 억제율은 ET 세포보다 IT 세포에서 더 컸다. 또한 Rilzole의 국소 적용은 ET 세포에서 지속 활성의 유지를 방해하였다. 이러한 결과는 $I_{Na,P}$ 크기의 차이가 ET 세포와 IT 세포 간 내재적 흥분성 차이에 기여함을 시사한다.

특정 세포군에서 내재적 흥분성 조절의 효과를 더 자세히 조사하기 위해서, IT 세포로 분류되는 피질-선조체(Cortico-striatal) PN을 연구대상으로 선정하였다. mPFC의 PN은 직접 및

간접경로의 중간 가시 뉴런(Direct pathway medium spiny neuron 과 Indirect pathway medium spiny neuron, 각각 dMSN 및 iMSN)에 글루타메이트 입력을 전달하고, 이 MSN의 불균형한 활동은 중독성 약물에 의한 보상관련 행동에 영향을 미친다. 중격의지핵 core(Nucleums accumbens core, NAcC)의 MSN으로 전달되는 전변연 피질(Prelimbic cortex, PL)로부터의 출력은 코카인에 의한 운동 민감성(Locomotor sensitization, LS)에 중요한 역할을 하지만, PL-NAcC 시냅스 가소성에 대한 연구는 미비한 실정이다. 이를 밝히기 위하여 본 연구는 유전자 변이 동물과 역행 추적 실험기법을 사용하여, 발현하고 있는 도파민 수용체를 기반으로 PL-NAcC PN을 분류하고 전기생리학적 특성을 관찰하였다. PL-NAcC 시냅스에서 코카인에 의해 유발된 변화를 조사하기 위해, NAcC MSN에서 PL PN의 신경 말단을 광자극하여 발생하는 EPSC 크기를 측정하였다. PL PN의 흥분성이 코카인에 의한 PN-NAcC 시냅스 가소성에 미치는 영향을 살피기 위하여 Riluzole을 사용하였다. 그 결과, NAcC로 투사하는 PL PN은 D1 수용체를 발현하는 그룹(D1-PN)과 D2 수용체를 발현하는 그룹(D2-PN)으로 구분되며, 이들의 흥분성이 각각의 도파민 작용제에 의해 상반되게 조절됨을 발견하였다. 일반적인 상황에서는 D1-, D2-PN 모두 dMSN 및 iMSN으로 고르게 신호를 전달하지만, 반복된 코카인의 투여는 D1-, D2-PN에서의 신호전달을 시냅스 전 메커니즘에 의존적으로 dMSN으로 치우치게 하였다. 본래 D2 수용체의 활성화는 D2-PN의 흥분성을 감소시켰지만, 그룹1 대사성 글루탐산 수용체(Metabotropic glutamate receptor)가 D2 수용체와 함께 활성화될 경우 D2-PN의 흥분성이 증가하였다. 코카인에 의한 PL-NAcC 연결의 재배선은 LS를 동반하였으나,

재배선과 LS는 PL 뉴런의 내재적 흥분성을 감소시키는 Riluzole을 PL에 주입할 경우 그 현상이 배제되었다. 이러한 결과는 코카인에 의해 유도되는 PL-NAcC 연결의 재배선이 LS와 잘 관련되어 있으며, 재배선 및 LS 가 PL 뉴런의 흥분성 감소로 예방될 수 있음을 나타낸다.

주요어 : 지속성 Na^+ 전류, 내측 전전두엽 피질, 전변연 피질, 중격의지핵, 보상회로, 전시냅스 가소성, 코카인 민감화

학 번 : 2014-22023